



HAL
open science

An analysis of nonlinearity effects on bedload transport prediction

A. Recking

► **To cite this version:**

A. Recking. An analysis of nonlinearity effects on bedload transport prediction. *Journal of Geophysical Research*, 2013, 118 (3), p. 1264 - p. 1281. 10.1002/jgrf.20090 . hal-00916417

HAL Id: hal-00916417

<https://hal.science/hal-00916417>

Submitted on 10 Dec 2013

HAL is a multi-disciplinary open access archive for the deposit and dissemination of scientific research documents, whether they are published or not. The documents may come from teaching and research institutions in France or abroad, or from public or private research centers.

L'archive ouverte pluridisciplinaire **HAL**, est destinée au dépôt et à la diffusion de documents scientifiques de niveau recherche, publiés ou non, émanant des établissements d'enseignement et de recherche français ou étrangers, des laboratoires publics ou privés.

1 **An analysis of nonlinearity effects on bedload transport prediction**

2 A. Recking, IRSTEA, UR ETGR, 2 Rue de la Papeterie, BP76, 38402 Saint Martin d'Hères,

3 France. E-mail: alain.recking@irstea.fr

4

5

6 **ABSTRACT**

7 Because bedload equations are nonlinear and because parameters describing the flow
8 and the bed can have large variance, different results are expected when integrating bedload
9 over a cross section with respect to spatially variable local data (2D), or when computing
10 bedload from cross-section-averaged data, which reduces the problem to uniform conditions
11 (1D). Evidence of these effects is shown by comparing 1D (flume-derived) equations with 2D
12 field measurements, and by comparing a 2D (field-derived) equation with 1D flume
13 measurements, leading to the conclusion that different equations should be used depending on
14 whether local or averaged data are used. However, whereas nonlinearity effects are
15 considerable for low-transport stages, they tend to disappear for higher flow conditions.

16 Probability distribution functions describing the variance in flow and bed grain size
17 distribution (GSD) are proposed and the width-integrated bedload data (implicitly containing
18 the natural variance in bed and flow parameters) are used to calibrate these functions. The
19 method consists of using a Monte Carlo approach to match the measured 2D bedload
20 transport rates with 1D computations, artificially reproducing the natural variance associated
21 with the mean input parameters. The Wilcock and Crowe equation was used for the 1D
22 computation because it was considered representative of 1D transport.

23 The results suggest that nonlinearity effects are mostly sensitive to the variance in
24 shear stress, modeled here with a gamma function, whose shape coefficient α was shown to
25 increase linearly with the transport stage. This variance in shear stress suggests that even for
26 very low flow conditions, shear stress can locally exceed the critical shear stress for the bed
27 armor, generating local armor break-up. This could explain why the bedload GSD is usually
28 very similar to subsurface GSD, even in the presence of complete armor.

29
30
31

32 INTRODUCTION

33 Bedload transport prediction is important for many applications, including river
34 engineering, hazard prediction, and environmental monitoring and management.
35 Sophisticated equations have been proposed in recent decades [*Parker, 1990; Wilcock and*
36 *Crowe, 2003*], and when the quality of the required input data is good and the flow hydraulics
37 are calculated in sufficient detail to take into account shear stress variations, they have been
38 shown to adequately predict transport rates, changes in bed topography, and downstream
39 fining [*Ferguson and Church, 2009*]. However, the requisite data (detailed grain size
40 distribution [GSD], topography, discharge or depth) are not always available, and in many
41 practical situations bedload must be computed with limited information and width-averaged
42 river characteristics: The GSD is reduced to a few surface diameters (D_{50} , D_{84}), often
43 estimated by surface counting [*Wolman, 1954*], the bed topography is assumed to be
44 trapezoidal or rectangular and reduced to a mean width W and slope S , and the flow is
45 considered uniform at the reach scale (a single water depth d for a given discharge and the
46 energy slope equal to the bed slope).

47 Despite reflecting the reality of many practical situations, the proposed approach of
48 computing bedload with simple models and width-averaged data has been widely criticized
49 for two main reasons: First, equations using limited input data are assumed to be incapable of
50 reproducing the full complexity of transport [*Habersack and Laronne, 2002*], and second,
51 since bedload equations are nonlinear with exponents that may exceed values of 10, width-
52 averaged bedload calculation has been suspected of under-estimating the true bedload flux if
53 there is any local and/or spatial variation in either the bed material size distribution or in the
54 flow hydraulics [*Gomez and Church, 1989; Paola and Seal, 1995; Ferguson, 2003; Bertoldi,*
55 *et al., 2009; Francalanci, et al., 2012*].

56 *Ferguson* [2003] demonstrated nonlinearity effects with an analytical model based on
57 the Meyer–Peter and Mueller formulation (derived for local transport in a flume). Using a
58 probability function describing the shear stress variation around its mean value, he showed
59 that additional flux locally induced by high shear stress outweighs the lower flux induced by
60 low shear stress and that, consequently, the total flux (the sum of all local fluxes) should be
61 higher than the flux computed with the averaged shear stress. These effects are illustrated in
62 Figure 1, where τ^* is the Shields number, which for diameter D is:

$$\tau^* = \frac{RS}{(s-1)D} \quad (1)$$

63 where R is the hydraulic radius, S is the slope, and $s=\rho_s/\rho$ is the ratio between the sediment
64 and the water density. Figure 1a illustrates a river section, the averaged Shields stress $\langle \tau^* \rangle$
65 and computed bedload transport $q_s(\langle \tau^* \rangle)$, and its decomposition in local values τ_i^* and
66 $q_s(\tau_i^*)$; whereas the local shear stress τ_i^* is twice the average value $\langle \tau^* \rangle$ in the figure, the
67 corresponding computed bedload transport is plotted such that $q_s(\tau_i^*) \gg 2q_s(\langle \tau^* \rangle)$. These
68 effects occur because bedload has been shown to be a power function of the shear stress and
69 the value of the exponent is greater than 1. Considering $q_s \propto \tau^{*p}$, Figure 1b shows that the
70 higher the value of the exponent p , the greater these effects (with a threshold equation of the
71 form $q_s \propto (\tau^* - \tau_c^*)^p$ these effects would be maximum near the critical Shields stress τ_c^*).

72 In contrast to the above expectation, most studies comparing bedload equations to
73 measured bedload transport rates report large over-estimates instead of under-estimates when
74 equations are used with width-averaged data, especially for gravel bed rivers [*Rickenmann*,
75 2001; *Barry, et al.*, 2004; *Bathurst*, 2007; *Recking, et al.*, 2012]. In addition, because
76 equations derived on the basis of field data are supposed to have a built-in allowance for the
77 effects of spatial variability, they should considerably improve the computation of bedload
78 transport when compared with standard 1D equations; however, many equations based on

79 field data are also site specific, and *Barry et al.* [2004; 2007] did not draw any conclusions
80 about the superiority of one category of equation when compared with field data.

81 Consequently, the questions this paper aims to answer are: How do the nonlinear
82 effects influence predicted transport rates? Can a single equation, used with either the exact
83 local shear stress or with width-averaged river characteristics, reproduce local transport and
84 width-averaged transport, respectively, or should we consider two distinct families of
85 equations, depending on whether bedload must be computed with local shear stress (as in
86 numerical models) or with width-averaged data? Can we relate nonlinearity effects to the
87 natural variance in flow and bed parameters?

88 First, flume and field data are presented. Secondly, they are used with several bedload
89 transport equations (1D capacity equation, 1D surface-based equation, and 2D field-derived
90 equation) to look for evidence of nonlinearity effects. Thirdly, the variance associated with
91 each flow and bed parameter is described, and a Monte Carlo approach is used for statistically
92 investigating (calibrating) the shape parameter of each probability distribution function.
93 Finally, the results are used to discuss the use of equations in field applications.

94 **DATA SET PRESENTATION**

95 In this part, the data set used in the analyses is presented; field data are considered 2D
96 data because they are width-integrated, and they are distinguished from flume data that are
97 considered 1D (near-uniform) and therefore an analogue for local transport in natural rivers.
98 Note that the term 1D should rigorously correspond to strictly uniform flows (constant depth
99 and bed roughness); however, such flows are almost never fully observed even in the flume,
100 where small bedforms can exist and sediment patches can develop [*Meyer-Peter and Mueller,*
101 1948; *Dietrich, et al.*, 1989]. Consequently 1D flow is used here to designate quasi-uniform
102 flows when compared with 2D flows in the field.

103 All parameters considered width-averaged are noted between the symbols <>; other standard
104 notations correspond to local values. The flow conditions were discriminated with the
105 transport stage defined by the τ^*/τ_c^* ratio [Church and Zimmerman, 2007], where τ_c^* is the
106 critical Shields stress estimated with the following formula fitted to a compilation of field data
107 from the literature [Recking, 2009]:

$$\tau_{ci}^* = (1.32S + 0.037) \left(\frac{D_i}{D_{50}} \right)^{-0.93} \quad (2)$$

108 Large uncertainties exist on τ_c^* [Buffington and Montgomery, 1997] and a constant and
109 arbitrary value $\tau_c^*=0.03$ [Parker, et al., 2003] or 0.047 [Meyer-Peter and Mueller, 1948]
110 could have been used, but using a dependency with slope is more likely to represent reality
111 [Mueller, et al., 2005; Lamb, et al., 2008; Recking, 2009; Ferguson, 2012]. The transport
112 stage can be defined for different diameters D_i . D_{50} was used because this diameter is often
113 considered representative. However, because the exponent in Eq. 2 is near 1, the results would
114 have been slightly changed with other diameters such as D_{84} (used for plotting the data in
115 Recking et al. 2012). Nonetheless, this is not important because this choice impacts only the
116 distribution of the results on the figures (the x-axes) and not the results themselves (all
117 equations being used exactly as recommended by their authors).

118 **1D data**

119 Investigating local transport assumes knowledge of the local values. Whereas a few
120 field data sets measure local transport and the associated flow velocity, the bed surface GSD
121 is always highly uncertain and always averaged at the reach scale. Such local data sets would
122 be very difficult to construct because measuring the local bed GSD associated with transport
123 is almost impossible during flooding. A practical way to obtain such information is flume
124 experiments, where the flow can be stopped and the bed can be sampled after each bedload
125 measurement, as done by Wilcock et al. [2001]. They produced bedload data in a 0.6-m-wide
126 and an 8-m-long tilting flume, with recirculation of poorly sorted sediment mixtures and flow

127 conditions allowing partial transport. Five runs were produced with different sand contents
128 and the data are summarized in Table 1 and are available in *Wilcock et al.* [2001]. These data
129 cover a large slope range (0.06%–2%) and are (to the best of the author’s knowledge) the only
130 published flume data that fully document partial transport [*Wilcock and McArdell*, 1993].
131 These flows are not strictly speaking 1D, as uniformity implies a perfectly constant water
132 depth and bed roughness. However, as mentioned by the authors, “*the sediment bed was*
133 *essentially planar,*” which allows for the hypothesis of near-uniform flows when compared
134 with flows in a natural river reach.

135 **2D data**

136 An existing field data set comprising 6,319 values (available in *Recking*, [2010]) was
137 expanded with new data from the literature comprising 2,614 measurements collected on 24
138 river reaches. The main characteristics of this new data set are given in Appendix A and the
139 data (including bed surface GSD) are available on-line as supplementary material. The
140 complete data set comprises 8,940 values collected at 109 river sites and is summarized in
141 Table 2. Most sampling results (when specified) provided width-averaged data for the bed
142 GSD, the flow characteristics (discharge, velocity), and the bedload transport. The following
143 figures provide general descriptions of the data set and were used in the subsequent
144 calculations of 2D bedload transport.

145 Figure 2 presents the cumulative distribution of diameter $\langle D_{84} \rangle$, slope $\langle S \rangle$, and width
146 $\langle W \rangle$ for the 109 reaches composing the data set. Only 5% are sand bed rivers and 10% have a
147 D_{84} smaller than 1 cm (not many published bedload data collected on sand bed rivers were
148 found in the literature); 70% are gravel bed rivers and 20% are cobble and boulder bed rivers.
149 Slopes span a broad range of values from 0.01 to 8%. Most widths are in the range 0–15 m,
150 but reaches as large as 500 m were also considered. The different ranges obtained for $\langle D_{84} \rangle$,
151 slope $\langle S \rangle$, and width $\langle W \rangle$ are consistent, with width and grain size evolving with slope, from

152 large lowland sandy rivers to steep narrow boulder streams [Montgomery and Buffington,
153 1997; Church and Zimmerman, 2007]. Figure 3 plots slope $\langle S \rangle$ as a function of $\langle D_{84} \rangle$ for
154 the data set considered; the trend roughly follows a power function.

155 A selection of 121 GSDs are plotted in Figure 4. Figure 4a plots a selection of 78
156 GSDs collected in gravel bed rivers (from the Idaho data set; King *et al.* [2004]) and the
157 corresponding averaged GSD. It shows a similar shape between all curves. Figure 4b plots 42
158 additional GSDs, including sand bed rivers. Figure 4 indicates that the sand fraction at the bed
159 surface $\langle F_s \rangle$ can vary greatly, and these data suggest $0 < \langle F_s \rangle < 0.2$ for most gravel bed
160 rivers. This is confirmed in Figure 5, where $\langle F_s \rangle$ is plotted as a function of $\langle D_{84} \rangle$: It is close
161 to 1 for sand bed rivers and rapidly decreases to approximately 0.1–0.15 for gravel bed and
162 cobble bed rivers.

163 Figure 6 (that also includes additional data from Pitlick *et al.*, [2008]) indicates that
164 the $\langle D_{84} \rangle / \langle D_{50} \rangle$ ratio is approximately equal to 2, which was also found to be representative
165 of gravel bed rivers by Rickenmann and Recking [2011] with another data set. However, the
166 ratio can also differ significantly from 2, and $\langle D_{84} \rangle / \langle D_{50} \rangle = 2$ is associated with a variance
167 following approximately a log-normal distribution with a standard deviation $\sigma_{D_R} = 0.3$ ($1.1 <$
168 $D_{84}/D_{50} < 3.3$).

169 Figure 7 presents relations between the transport stage and the bed surface $\langle D_{84} \rangle$ and
170 the slope. It indicates a decrease of $\langle \tau^* \rangle / \langle \tau_c^* \rangle$ with $\langle D_{84} \rangle$ following roughly a power law
171 ($R^2=0.45$); a similar relation does not seem to exist with the slope. Low $\langle \tau^* \rangle / \langle \tau_c^* \rangle$ values for
172 high $\langle D_{84} \rangle$ values is not surprising, as the Shields number $\langle \tau^* \rangle$ is known to barely exceed
173 120% of the critical value $\langle \tau_c^* \rangle$ in gravel bed rivers [Parker, 1978; Andrews, 1983; Ryan, *et*
174 *al.*, 2002; Mueller, *et al.*, 2005; Parker, *et al.*, 2007]. In fact, only for sand and fine gravels
175 can the transport stage be very high [Buffington, 2012].

176 Figure 8a plots the unit transport rates $\langle q_s \rangle$ (g/s/m) and Figure 8b plots the averaged
177 dimensionless transport $\langle \Phi \rangle$, with Φ defined by [Einstein, 1950]:

$$\Phi = \frac{q_s}{\rho_s \sqrt{g(s-1)D_{50}^3}} \quad (3)$$

178 where ρ_s is the sediment density. Transport rates cover a wide range; it is interesting to note
179 that the threshold value $\langle \tau^* \rangle / \langle \tau_c^* \rangle = 1$ (computed for D_{50}) corresponds to somewhat
180 considerable transport and $\langle \tau^* \rangle / \langle \tau_c^* \rangle = 2$ approximately delimits two groups with a change in
181 trend, a result which is consistent with previous analyses [Parker, et al., 1982; Buffington,
182 2000].

183 To complete this description of the field data, the bed morphology should be
184 presented. Unfortunately, except for a few cases [Hassan and Church, 2001; Church and
185 Hassan, 2002], an exact description of the reach used for measurements was usually not
186 included in the publications. Mostly only general descriptions of river morphology were
187 provided, but available information suggests that straight reaches were frequently chosen for
188 bedload measurements. Nevertheless, the surrounding reach morphology of some sites may
189 exhibit substantial topographic variation (e.g., pool-riffle or step-pool channels).

190 **LOOKING FOR EVIDENCE OF NONLINEARITY EFFECTS**

191 In this part, the flume and the field data are used with bedload equations to look for
192 evidence of nonlinearity effects. Bedload equations are used exactly as recommended by their
193 authors.

194 ***From the flume to the field***

195 This part aims to analyze whether averaging the data produces under-prediction when
196 1D equations are used in the field.

197 Sixteen flume-derived 1D bedload transport equations were compared with a large
198 field data set in Recking et al. [2012]. The conclusion of this study was that for the lowest
199 transport stages (corresponding to partial transport, with $\tau^* / \tau_c^* < 1$ for the coarser fractions),

200 these threshold equations predicted zero transport whereas the measured transport was non-
201 zero. When the non-zero transport computations were considered, the results showed over-
202 estimation, for all equations, often by several orders of magnitude, which is not in accordance
203 with the expected under-estimation induced by nonlinearity. This resulted in a generally poor
204 performance of most of the equations tested, except for high flow conditions (when $\tau^*/\tau_c^* > 2$,
205 which corresponds to sand and fine gravels in Figure 7a). One reason potentially responsible
206 for over-prediction is that these equations do not account for the changing critical shear stress
207 with slope.

208 To overcome this threshold problem (zero prediction and slope effects), a 1D bedload
209 equation expressed as a function of τ^*/τ_c^* was fitted in *Recking* [2010] on a large flume data
210 set obtained with near-uniform sediments (compilation comprising most of the data that have
211 served to build the equations reported in the literature, available as supplementary material in
212 *Recking*, [2010]). This equation accounts for variation of the critical Shields stress with slope
213 and is presented in Appendix B1. When this 1D equation (used with the median diameter) is
214 compared with the 1D flume data from *Wilcock et al.* [2001], the results plotted in Figure 9
215 can be deemed satisfying, considering that there was no calibration; most particularly, the
216 trend is very good and there is no clear evidence for over- or under-prediction.

217 On the other hand, when this equation is compared with the field data, the results
218 plotted in Figure 10 clearly confirm under-prediction when the transport stage is $\tau^*/\tau_c^* < 0.7$,
219 as expected by nonlinearity effects. However, like the other equations tested in *Recking et al.*
220 [2012], this equation over-estimates transport rates for higher flow conditions and gives
221 acceptable results only when $\tau^*/\tau_c^* > 2$ approximately. The possible reason for over-
222 estimation in the range $0.7 < \tau^*/\tau_c^* < 2$ is that all these equations were derived to match as
223 well as possible the transport capacity of nearly uniform fine materials in flume experiments
224 (see *Recking et al.* 2008 for a review of these data). In these conditions, each increment in

225 shear stress was systematically balanced by an increment in transport. In gravel and cobble
226 bed rivers, sediments are not always available for transport because of supply limitations and
227 hiding effects, and small increments in shear stress may not be compensated by an immediate
228 increment in bedload, which can explain over-estimation [Bathurst, 2007; Recking, 2012].
229 The results are improved in the range $1 < \tau^*/\tau_c^* < 2$ when the Meyer–Peter and Mueller [1948]
230 shear stress correction is used; however, it also considerably increases under-prediction in the
231 $\tau^*/\tau_c^* < 1$ range.

232 To overcome the above-mentioned problem, fractional equations were developed for
233 computing the transport of what is actually present on the bed surface [Parker and
234 Klingeman, 1982; Parker, 1990; Wilcock and Crowe, 2003]. Among these equations, the
235 Wilcock and Crowe [2003] equation is considered a truly surface-based relation [Parker,
236 2009] because it was derived from the flume experiments of Wilcock *et al.* [2001], with the
237 exact surface GSD being measured immediately after each flow event. This equation
238 (presented in Appendix B2) was used as suggested by the authors, with the GSDs sampled at
239 $1-\psi$ intervals, and by computing the grain shear stress with $\tau = 17(SD_{65})^{1/4}U^{3/2}$ [Wilcock, *et*
240 *al.*, 2009]. A comparison with the field data set (restricted to 82 reaches and 6,239 values
241 because the full GSD was not available for all data) showed no significant over-prediction and
242 a tendency for under-prediction at low shear stresses, in agreement with expected nonlinearity
243 effects (Figure 11). Similar results were obtained by Gaeuman *et al.* [2009] who compared
244 the Wilcock and Crowe equation to bedload measurements of the Trinity river.

245 To conclude, the above analysis suggests that the variance in flow and bed parameters
246 produces under-prediction at low transport stages when 1D equations are used in the field.

247 ***From the field to the flume***

248 A second way to verify the effects of nonlinearity is to use a 2D field-derived equation
249 for computing local transport. By fitting the width-integrated transport measurements, these

250 equations have a built-in allowance for the effects of spatial variability, which should improve
251 the computation of field bedload transport with width-averaged input data, when compared
252 with standard 1D equations. On the other hand, if they implicitly compensate for spatial
253 variability, these equations should logically over-predict transport when compared with 1D
254 measurements because of nonlinearity effects. This is what was tested here by comparison
255 with the flume data from *Wilcock et al.* [2001] (assuming that these data are representative of
256 1D transport in the field).

257 Several 2D field-derived equations have been proposed in the literature [*Parker, et al.*,
258 1982; *Barry, et al.*, 2008; *Recking*, 2010]. Here, an equation (presented in Appendix B3)
259 proposed in a previous paper by the author [*Recking*, 2013] was used because it requires only
260 a few parameters and permits a direct comparison with flume data. This equation was
261 compared with the field data set (restricted to 5,735 values not used in its construction,
262 collected at 73 sites, for blind testing), and the results plotted in Figure 12 indicates only a
263 slight under-prediction at very low Shields stress ratios. The comparison with a selection of
264 river reaches did not indicate any particular dependency on the bed morphology (Figure 13).
265 On the other hand, the comparison with 1D flume data confirmed over-prediction for the low
266 transport stages, as expected by nonlinearity effects (Figure 14).

267 To conclude this part, only low transport stages are affected by nonlinearity effects.
268 Assuming that the flume data are representative of local flows, this analysis suggests that the
269 variance in flow and bed parameters produces under-prediction when 1D equations are used
270 in the field. Field-derived equations compensate for these effects, but by contrast they over-
271 predict bedload transport when they are used for computing local transport with local flow
272 values (e.g., in a numerical model). The following section aims to fill the gap between 1D and
273 2D transport by investigating the variance associated with each parameter.

274

275 INVESTIGATING THE MISSING DIMENSION

276 The difference between 1D bedload computation and 2D bedload measurements
277 results from variance in shear stress and bed properties. Each bedload value of the data set is
278 by construction the average of several bedload values measured locally and produced by the
279 variance in flow and bed GSD (as illustrated in Figure 1a); consequently, bedload data
280 implicitly include the variance in flow and bed parameters, which evolve in both space and
281 time. On the other hand, this variance is absent from the associated flow and bed data
282 (discharge measured not simultaneously and often at a gauging station, in another location,
283 and with a single mean GSD). This variance, which is present in bedload data and absent in
284 the flow and bed data used in the equations, is what *Ferguson* [2003] called the “missing
285 dimension.”

286 The only way to make the use of a 1D equation consistent for comparison with
287 measured 2D field data would be to “artificially” reproduce the natural flow and bed
288 variability. This is done in this part of the paper, using the averaged input data in the 1D
289 Wilcock and Crowe equation, with their variance described by probability distribution
290 through a Monte Carlo approach.

291 *Probability distribution functions describing the variance in flow and bed parameters*

292 The depth $\langle d \rangle$ can vary considerably in an irregular cross section, ranging from near
293 zero close to the banks to a maximum at the thalweg, and is linearly related to shear stress for
294 a given slope $\langle \tau \rangle \propto \langle S \rangle \langle d \rangle$. The variance associated with longitudinal slope across a given
295 cross section is difficult to evaluate; however, as pointed out by *Ferguson* [2003], available
296 field studies have actually shown a positive correlation between d and τ (local deviations from
297 $\tau \propto d$ tending to cancel each other out), leading to a similar frequency distribution for d and τ .
298 This is why in the following the variance was considered directly for the shear stress $\langle \tau \rangle$
299 instead of separate variance for $\langle d \rangle$ and $\langle S \rangle$. This variance was described with an

300 asymmetric gamma probability function, as already proposed in other works [Paola, 1996;
301 Nicholas, 2000; Bertoldi, et al., 2009]:

$$p(\tau) = \frac{\alpha^\alpha \hat{\tau}^{\alpha-1} e^{-\alpha\hat{\tau}}}{\langle\tau\rangle\Gamma(\alpha)} \quad (4)$$

302 where $\hat{\tau} = \tau/\langle\tau\rangle$, $\langle\tau\rangle$ is the width-averaged bed shear stress, and α is a parameter describing
303 the width of the distribution. The lower its value, the larger the variance in τ . A value $\alpha=1$
304 was found to be a limiting value for highly irregular cross sections [Paola, 1996; Nicholas,
305 2000], for instance, in braided streams. It also predicts a shear stress in the range $0 < \tau/\langle\tau\rangle <$
306 5 (Figure 15), which is approximately what Ferguson [2003] obtained with his probability
307 function when the shear stress is below its mean value of over 80% of the cross section.
308 Values greater than 5 would be representative for single-thread irregular channels, and α
309 tends toward infinity for a rectangular cross section.

310 Fractional equations require a complete definition of the GSD. Instead of discussing
311 the variance associated with each size class, GSD was reduced to three parameters: the sand
312 fraction on the bed surface F_s , the median diameter D_{50} , and the D_{84}/D_{50} ratio. This model,
313 presented in Table 3, was obtained by considering the proportionality ratios between each size
314 class measured in the compilation of 78 GSDs, plotted in Figure 4a. Figure 16a shows three
315 examples of measured GSDs and their approximation with the model, and Figure 16b and c
316 indicates that the difference between the measured and computed percentage for each fraction
317 of the whole data set is very weak. There is no intention here to reduce all natural GSDs to
318 these three parameters, but it allows very realistic GSDs to be built.

319 Only a few studies have investigated the variability of GSDs in a given reach [Church
320 and Kellerhalls, 1978; Crowder and Diplas, 1997], and defining the variance for F_s , D_{50} , and
321 D_{84}/D_{50} for the purpose of this study is not trivial. Considering the central limit theorem, the
322 distribution of the means of a series of samples should be normally distributed regardless of
323 the underlying distribution of the sample; therefore it is hypothesized that for a given mean

324 value $\langle D_{50} \rangle$, diameters D_{50} vary randomly following a normal distribution (Figure 17).
325 Several values were considered for standard deviation σ_D . The value $\langle D_{84} \rangle / \langle D_{50} \rangle = 2$ and the
326 associated normal distribution ($\sigma_{Dr} = 0.3$) observed between sites (Figure 6) was hypothesized
327 as always valid, including for different locations in a given site. $F_s = 0.1$ was considered on
328 average for gravel bed rivers (Figure 5); however, sand can be either uniformly distributed
329 over the surface or concentrated in local patches [Buffington and Montgomery, 1999a;
330 Dietrich, et al., 2006], which can be described with an asymmetric beta function $B(x_1, x_2)$,
331 with an average set to $x_1/x_2 = 0.1$ (where x_1 and x_2 are the shape parameters of the function).
332 Figure 18 plots $B(x_1, x_2)$ for different values of x_1 and x_2 . Low coefficients ($x_1 = 0.001$; $x_2 =$
333 0.01) simulate near-zero sand everywhere and high local sand concentration (patches); on the
334 other hand, high coefficients ($x_1 = 100$ and $x_2 = 1000$) simulate a more uniform distribution of
335 the sand fraction over the surface.

336 Limited evidence of a clear correlation between grain size and depth led Ferguson
337 [2003] to consider two limiting scenarios: purely random patchiness, and perfect fining
338 upward as in classic models of meander point bars. Here, only the case of near-straight
339 reaches was considered, with no or little correlation between grain size and depth. Flows over
340 typical morphological units such as riffle, pools, and bars are considered in the discussion.

341 ***A Monte Carlo approach for calibrating the probability functions***

342 In this section the width-integrated bedload data (implicitly containing the natural
343 variance in bed and flow parameters) were used to calibrate the probability functions
344 describing the variance in flow and bed parameters. This approach is in a sense similar to that
345 of Chiari and Rickenmann [2010], who used bedload measurements for back-calculating the
346 macro roughness of several alpine rivers; however, whereas they used a numerical model, a
347 Monte Carlo approach was used here.

348 For a given set of width-averaged input data (say, $\langle F_s \rangle, \langle D \rangle, \langle \tau \rangle$), the Monte Carlo
349 approach consists in performing a large number of random draws from the probability
350 distribution of each input parameter to construct numerous sets of local values (F_s, D, τ)
351 about the means. In the second step, each set of local values is used in the 1D bedload
352 equation to compute the associated local bedload transport q_s . Assuming the probability
353 distribution functions are correct, averaging these local bedload values $\frac{1}{N} \sum_N q_s$ should
354 retrieve (in a statistical sense) the measured (and width-averaged) bedload transport $q_{s \text{ meas}}$.

355 For each flow range (considered through the ratio $\langle \tau^* \rangle / \langle \tau_c^* \rangle$) and given values of $\langle S \rangle$,
356 $\langle F_s \rangle$, $\langle D_{50} \rangle$, and $\langle D_{84} \rangle / \langle D_{50} \rangle$, the different steps are:

357 (1) computation of $\langle \tau^* \rangle$ for each transport stage $\langle \tau^* \rangle / \langle \tau_c^* \rangle$ (considered for values 0.3, 0.5,
358 0.7, 1, 1.3, 1.5, 2, 5, and >5) knowing $\langle \tau_c^* \rangle$ (given by Eq. 2), from which we deduce
359 $\langle R / D_{84} \rangle = 1.65 \langle \tau^* \rangle / \langle S \rangle$ (Eq. 1);

360 (2) calculation of the flow velocity $\langle U \rangle$ for $\langle R / D_{84} \rangle$ with the *Ferguson* [2007] flow
361 resistance equation (this equation was chosen because it has been shown to give satisfying
362 values when compared with a large data set in *Rickenmann and Recking*, [2011]);

363 (3) calculation of the appropriate mean grain shear stress $\langle \tau \rangle = 17 (\langle S \rangle \langle D_{65} \rangle)^{1/4} \langle U \rangle^{3/2}$
364 [*Wilcock, et al.*, 2009]; $\langle D_{65} \rangle$ is given in millimeters and deduced from the model of Table 3;

365 (4) construction of several sets of local values for τ and GSD (with the model of Table 3) by
366 random draws in the probability distributions of $\langle \tau \rangle$ and $\langle F_s \rangle, \langle D_{50} \rangle, \langle D_{84} / D_{50} \rangle$;
367 computation of the associated bedload $q_s(\tau, GSD)$ with the *Wilcock and Crowe* equation.

368 Large data sets ($N=5,000$) were constructed to ensure a stable solution for the computed
369 bedload probability distribution;

370 (5) calculation of the average value $\langle q_s(\tau, GSD) \rangle = \frac{1}{N} \sum_N q_s(\tau, GSD)$;

371 (6) comparison of $\langle q_s(\tau, GSD) \rangle$ with $q_{s\text{ meas}}$.

372 **Results of simulations**

373 The simulations were tested with different values for α (for τ), σ_D (for D_{50}), and x_1
374 (with $x_2 = 10x_1$ for $\langle F_s \rangle = 0.1$). Figure 19 compares the $q_s(\langle \tau^* \rangle) / q_{s\text{ meas}}$ ratios (where $q_{s\text{ meas}}$
375 is the measured bedload transport and $q_s(\langle \tau^* \rangle)$ is bedload computed with the Wilcock and
376 Crowe equation used with average input data, as shown in the right panel of Figure 11) with
377 $q_s(\langle \tau^* \rangle) / \langle q_s(\tau^*) \rangle$, where $\langle q_s(\tau^*) \rangle$ is the average bedload deduced from the Monte
378 Carlo computation. Adequate probability distributions should make it possible to fit
379 $\langle q_s(\tau^*) \rangle$ with $q_{s\text{ meas}}$ (in a statistical sense).

380 No stable solution could be obtained with $\sigma_D > 0.3$ (leading to near-zero D_{50}), and
381 simulations were considered with $0.1 < \sigma_D < 0.3$. This range is consistent with *Segura et al.*
382 [2010], who measured σ_D in the range 0.1–0.36 on the basis of multi-pebble counts [*Wolman,*
383 1954] involving 2,500–4,700 particles on three reaches of the Williams Fork River (Colorado,
384 USA). It is also consistent with measurements made on a large gravel bar on the Gunnison
385 River [*Barkett, 1998*], a tributary to the Colorado River, consisting of 28 separate Wolman
386 counts of 100 particles each (total of 2,800 particles), and for which σ_D was 0.28 (*John*
387 *Pitlick*, personal communication).

388 Figure 19a shows that it was not possible to match the measurements for all flow
389 conditions when setting a constant α -value ($\alpha = 1$ actually seems to work fairly well as a
390 lower limit to the data). As a consequence, α was empirically varied with the transport
391 stage $\langle \tau^* \rangle / \langle \tau_c^* \rangle$ in Figure 19 b and c. All combinations (α, σ_D, x_1) were tested with $\langle \tau^* \rangle / \langle \tau_c^* \rangle$
392 within the range [0.3–100], for constant slopes $\langle S \rangle$ and $\langle D_{50} \rangle$ (Figure 19b) and also with the

393 transport stage $\langle \tau^* \rangle / \langle \tau_c^* \rangle$ linked to the slope and GSD (Figure 19c) through relations plotted
394 in Figure 3 and Figure 7a. Whatever the hypothesis, the best fit between computed (with the
395 Monte Carlo approach) and measured bedload was obtained by varying α linearly with a
396 function given in the form (Figure 19b and c):

$$\alpha = \xi \frac{\langle \tau^* \rangle}{\langle \tau_c^* \rangle} \quad (5)$$

397 The value of ξ in Equation 5 is slightly sensitive to the variance in GSD. A value of 5 best fits
398 the measured bedload transport with $\sigma_D = 0.1$ (Figure 19c), and a value of approximately 8–10
399 (not shown in the figure) would be more appropriate for a higher variance in D_{50} ($\sigma_D = 0.25$).
400 Results plotted in Figure 19c indicate a weak dependency on whether sand is considered
401 uniformly displayed over the surface ($x_1=100$, $x_2=1000$) or is concentrated into patches
402 ($x_1=0.001$, $x_2=0.01$).

403 The conclusion from these simulations is that predictions are weakly sensitive to the
404 variance in GSD (Figure 19 b and c) but very sensitive to the variance in shear stress (Figure
405 19a). Such an increase in the parameter α with flow strength was an expected result
406 [Nicholas, 2000], and values within the range $2 < \alpha < 10$ are consistent with results for single-
407 thread channels found by *Tunncliffe et al.* [2012].

408 **DISCUSSION**

409 ***Consequences for field application***

410 The above results suggest that all models are not adapted to all situations. 1D
411 equations used with width-average input data are likely to under-estimate width average
412 bedload transport. The Monte Carlo approach (used with appropriate probability distributions)
413 can be used for compensating the “missing dimension.” It is illustrated hereafter with the
414 example of the Lochsa River (using hydraulics and bedload data presented in *King et al.*
415 [2004]).

416 For the given bed characteristics ($F_s=0.03$, $D_{50}=0.126$ m, $D_{84}=0.28$ m, $S=0.0023$), the
417 procedure has consisted in defining, for each of the 71 runs characterized by a measured
418 velocity U and depth d , the transport stage $\langle \tau \rangle / \langle \tau_c \rangle$, the GSD, the probability distribution for
419 all parameters (no calibration was used here, and $\alpha=5$, $\sigma_D=0.1$, $\sigma_{DR}=0.3$, $x_1=100$ and $x_2=1,000$
420 following the above results), and in building bedload data with the Wilcock and Crowe
421 equation (3,000 values were computed for each run), which were averaged and compared with
422 the measured bedload.

423 The results presented in Figure 20 indicate that taking into account the variance in bed
424 and flow parameters can greatly improve prediction when compared with a direct
425 computation of the width-averaged data. The inconvenience of this approach is that thousands
426 of calculations are needed for each width-averaged input data considered.

427 ***Local vs. averaged shear stress***

428 Testing the equations (Figure 11) and the Monte Carlo results (Figure 19) showed that
429 the under-prediction is greater for low transport stages and decreases with increasing shear
430 stress, as *Ferguson* [2003] also concluded. This can be explained by a reduced variance in the
431 shear stress when the flow increases, because depth variations with the local bed topography
432 may become relatively negligible with regard to the mean flow depth (this is particularly true
433 for moveable beds becoming flatter with increasing transport stage).

434 Equations 4 and 5 were used to compute the distribution of the local transport stage
435 $\tau / \langle \tau_c \rangle$, for different values of the mean transport stage $\langle \tau \rangle / \langle \tau_c \rangle$. The results, plotted in
436 Figure 21, indicate that for $\langle \tau \rangle / \langle \tau_c \rangle$ ratios as low as 0.3, the shear stress may locally be
437 higher than the critical shear stress for mobility of the bed surface ($\tau / \tau_c > 1$). This means that
438 local armor break-up can always exist to some degree, exposing the subsurface material to the
439 flow. This finding is consistent with the observation that even in the presence of a coarse
440 armor, with a zero sand fraction at the bed surface ($F_s = 0$), the bedload GSD is always much

441 finer than the surface GSD and equivalent to the subsurface GSD. This was, for instance, the
 442 case for several of the Idaho streams [King, et al., 2004], for which bedload was measured for
 443 very low transport stages. However, the bedload material may also include upstream sediment
 444 supply that is not accounted for in the current analysis. Consequently, the sand fraction
 445 measured at the bed surface at rest could be an incorrect indicator of sediment availability for
 446 bedload computation.

447 ***Several questions to be investigated further***

448 The first question is how much are the above results dependent on the Wilcock and
 449 Crowe equation, used here as representative of 1D transport? To answer this question, another
 450 1D equation was considered. In work not shown here, an attempt was made to adapt the 2D
 451 Recking [2013] equation (Appendix B3) to 1D transport by introducing a correction
 452 coefficient $\zeta < 1$ such that:

$$\Phi_{1D} = \zeta(\tau^*, F_s) \Phi_{2D} \quad (6)$$

453 According to Figure 14, the function $\zeta(\tau^*, F_s)$ must converge to 1 when the sand fraction F_s
 454 converges to 1 or when the transport value is high (when all grain classes are moving, which
 455 can be expressed, for instance, with reference to the threshold conditions τ_c^* for the coarser
 456 fraction considered through diameter D_{84} in Eq. 2). Calibration with the Wilcock et al. flume
 457 data gave:

$$\zeta(\tau^*, F_s) = \begin{cases} \left[1 + (0.15 \sqrt{\frac{\tau_c^*}{\tau^*}} - 0.12) \ln(F_s) \right]^{10} & \text{for } \tau^*/\tau_c^* < 1.56 \\ \zeta(\tau^*, F_s) = 1 & \text{for } \tau^*/\tau_c^* > 1.56 \end{cases} \quad (7)$$

458 where τ^* and τ_c^* were calculated with Eqs. 1 and 2 for $D_i = D_{84}$. This function performed as
 459 well as the Wilcock and Crowe equation for the bulk bedload transport when compared with
 460 the flume data of Wilcock et al., it produced results that are very similar to Figure 11 when
 461 compared with the field data, and gave a very similar result for α (i.e., linear variation with
 462 $\langle \tau^* \rangle / \langle \tau_c^* \rangle$) when used in the Monte Carlo approach. Consequently, it is not the Wilcock and

463 Crowe equation that should be questioned here, but the flume data from which it was derived:
464 Are they representative of local transport in the field? Very precise local field measurements
465 would be needed to confirm these results, not only for the bed shear stress and bedload
466 transport, but also for the associated bed surface GSD (such data do not yet exist to the best of
467 the author's knowledge).

468 A second question concerns the effects of the local bed morphology. The case of near-
469 straight reaches was considered here, with no or little correlation between the depth and GSD.
470 Developing probability functions that are typical of morphological units such as riffle, pools,
471 and bars [*Buffington and Montgomery, 1999b; Bunte and Abt, 2001*] may necessitate a more
472 sophisticated approach, linking these two parameters [*Ferguson, 2003*]. However,
473 investigating the correlation between depth and grain size is challenged by uncertainties on
474 the variance in GSDs, which may change with hydraulic roughness [*Buffington and*
475 *Montgomery, 1999a*] or other external factors, such as the transport stage: The streambed
476 textures are typically documented at low flow when the bed is at rest and likely reflect
477 preferential transport by secondary flows, during hydrograph recession. For instance, there is
478 no reason why the bed patchiness measured on the bed at rest would be representative of the
479 bed during flooding.

480 To conclude, the investigation proposed in this paper considered variations around the
481 mean input values, which themselves were assumed to be exact. However, an erroneous
482 estimation of the width-averaged input data is likely to strongly impact the results. This aspect
483 should be considered in further analysis. It should be noted that the Monte Carlo analysis can
484 also be a useful tool for estimating the error on bedload prediction, with consideration of
485 uncertainties attached to the measured (or estimated) field data [*Wilcock, et al., 2009*].

486 **CONCLUSIONS**

487 Because they are nonlinear, bedload transport equations should logically under-predict

488 observed bedload transport when they are used with averaged (flow and bed) input data
489 [*Gomez and Church*, 1989; *Paola and Seal*, 1995; *Ferguson*, 2003; *Bertoldi, et al.*, 2009;
490 *Francalanci, et al.*, 2012]. However, this expectation has not been clearly demonstrated in
491 prior studies comparing predicted transport rates with observed values, which show over-
492 prediction, usually by several orders of magnitude [*Rickenmann*, 2001; *Barry, et al.*, 2004;
493 *Bathurst*, 2007; *Recking, et al.*, 2012].

494 In this paper, evidence of nonlinearity was shown by comparing 1D (flume-derived)
495 equations and 2D field measurements (Figure 10, Figure 11) and by comparing a 2D (field-
496 derived) equation with 1D flume measurements (Figure 14). Comparison with a 1D
497 nonthreshold equation derived for uniform sediments [*Recking*, 2010] and with no shear stress
498 correction produced under-prediction for low transport stages only (when $\tau^*/\tau_c^* < 1$), over-
499 prediction in the range $1 < \tau^*/\tau_c^* < 2$, and near adequate transport for higher transport stages
500 (Figure 10). Over-prediction in the range $1 < \tau^*/\tau_c^* < 2$ is typical of other 1D threshold
501 equations [*Recking, et al.*, 2012]. The nonthreshold fractional equation from Wilcock and
502 Crowe used with shear stress correction also under-predicted bedload for the low transport
503 stages (when $\tau^*/\tau_c^* < 1$) as expected by nonlinearity effects, and adequately reproduced
504 bedload for higher transport stages (Figure 11). On the other hand, the field-derived 2D
505 equation [*Recking*, 2013] that implicitly takes into account the variance in flow and bed
506 parameters correctly predicted the field data but over-predicted 1D bedload transport
507 measured in the flume by *Wilcock et al.* [2001] (Figure 14).

508 Under-prediction exists because each bedload data is by construction the average of
509 several local bedload values containing the variance in shear stress and bed GSD, whereas
510 such variance is absent from the mean input values used in bedload equations. The GSD was
511 reduced to three parameters (F_s , D_{50} , D_{84}/D_{50}) and probability distribution functions were
512 proposed to describe the variance associated with the flow and the bed. Then the Wilcock and

513 Crowe equation was compared with the field bedload data in a Monte Carlo approach, in
514 order to calibrate the parameters of these functions. The conclusion is that bedload prediction
515 is weakly sensitive to the variance in bed GSDs but is highly sensitive to the variance in shear
516 stress (Figure 19). The shear stress was modeled by a gamma function, whose shape
517 coefficient was found to vary linearly with the transport stage $\langle \tau^* \rangle / \langle \tau_c^* \rangle$. The variance in
518 shear stress suggests that local shear stress can exceed the critical shear stress for the bed
519 armor even for very low flow conditions (Figure 21); this may explain local armor break-up
520 and why the bedload GSD is frequently equivalent to the subsurface GSD (much finer than
521 the surface GSD).

522 Several aspects of this study remain to be investigated. In particular, little is known
523 about the variance in GSDs for a given reach, and new data (collected in the flume or in the
524 field) are needed for comparison with the Wilcock et al. [2001] data used here as
525 representative of 1D transport.

526

527 **ACKNOWLEDGMENTS**

528 This study was supported by Irstea and the ANR GESTRANS project granted to the author. It
529 would not have been possible without the USDA and the USGS data sets, as well as all the
530 other published data sets presented in Recking [2010]. The author is particularly grateful to
531 Mary-Ann Madej from the USGS, Randy Klein from Redwood National and State Parks,
532 Dieter Rickenmann from WSL, Mike Church from UBC, Ian Reid from Loughborough
533 University, Sandra E. Ryan-Burkett from the US Forest Service, John Pitlick from Boulder
534 University, and François Métivier from IPGP for having generously and spontaneously agreed
535 to share their data. The author would also like to thank Rob Ferguson, Mike Church and other
536 anonymous reviewers who greatly contributed to this paper by providing helpful reviews of
537 an earlier version of this manuscript. Thanks are extended to John Buffington (Associate
538 Editor), who contributed to this paper by providing additional reviews. Special thanks are
539 addressed to John Pitlick for discussions and very helpful comments.

540

541 **FIGURE CAPTIONS**

542 Figure 1: Schematic representation of nonlinearity effects on a river cross section. Figure 1a
543 illustrates a river section, its averaged parameters $\langle \tau^* \rangle$ and $q_s(\langle \tau^* \rangle)$, and its decomposition
544 in local values τ_i^* and $q_s(\tau_i^*)$; Figure 1b indicates that the higher the value of the shear stress
545 exponent, the greater the nonlinearity effects.

546

547 Figure 2: Cumulative distribution of $\langle D_{84} \rangle$, slope $\langle S \rangle$, and width $\langle W \rangle$, for the field data set
548 (109 reaches)

549

550 Figure 3: Variation of the slope $\langle S \rangle$ with $\langle D_{84} \rangle$ deduced from the field database

551

552 Figure 4: Grain size distributions for the field data set: (a) a selection of 78 GSDs from gravel
553 bed rivers; (b) additional data (43 GSDs) including sand bed rivers

554

555 Figure 5: Plot of the sand fraction F_s as a function of the bed surface D_{84}

556

557 Figure 6: D_{84}/D_{50} ratio measured for a selection of 170 river reaches (left) and associated
558 probability distribution function (right)

559

560 Figure 7: Relationship between the transport stage $\langle \tau^* \rangle / \langle \tau_c^* \rangle$ and the bed surface $\langle D_{84} \rangle$ and
561 the slope $\langle S \rangle$

562

563 Figure 8: Transport rates plotted as a function of the transport stage $\langle \tau^* \rangle / \langle \tau_c^* \rangle$; (a) unit
564 transport $\langle q_s \rangle$ (g/s/m); (b) dimensionless transport (Einstein parameter $\langle \Phi \rangle$)

565

566 Figure 9: Comparison of the *Wilcock et al.* [2001] data ($q_{s \text{ meas}}$) with the *Recking* [2010]
567 equation ($q_s(\langle\tau^*\rangle)$; Appendix B1), which represents a best fit of flume data having near-
568 uniform sediments

569

570 Figure 10: Comparison of the field data ($q_{s \text{ meas}}$) with the *Recking* [2010] equation ($q_s(\langle\tau^*\rangle)$;
571 Appendix B1), which represents a best fit of flume data having near-uniform sediments:
572 measured unit bedload $q_{s \text{ meas}}$ vs. computed value $q_s \langle\tau\rangle$ (left panel), and $q_{s \text{ meas}} / q_s \langle\tau\rangle$ ratio
573 vs. transport stage (right panel).

574

575 Figure 11: Comparison of the field data ($q_{s \text{ meas}}$) with the Wilcock and Crowe equation [2003]
576 ($q_s(\langle\tau^*\rangle)$; Appendix B2): measured unit bedload $q_{s \text{ meas}}$ vs. computed value $q_s \langle\tau\rangle$ (left panel),
577 and $q_{s \text{ meas}} / q_s \langle\tau\rangle$ ratio vs. transport stage (right panel).

578

579 Figure 12: Comparison of the field data ($q_{s \text{ meas}}$) with the field equation [*Recking*, 2010;
580 2013] ($q_s(\langle\tau^*\rangle)$; Appendix B3): measured unit bedload $q_{s \text{ meas}}$ vs. computed value $q_s \langle\tau\rangle$ (left
581 panel), and $q_{s \text{ meas}} / q_s \langle\tau\rangle$ ratio vs. transport stage (right panel).

582

583 Figure 13: Performance of the field equation [*Recking*, 2013; Appendix B3] across a broad
584 range of grain size and channel morphology

585

586 Figure 14: Comparison of the *Wilcock et al.* [2001] data ($q_{s \text{ meas}}$) with the field equation
587 [*Recking*, 2010; 2013] ($q_s(\langle\tau^*\rangle)$; Appendix B3); F_s is the sand fraction at the bed surface

588

589 Figure 15: Gamma function of $\tau/\langle\tau\rangle$ plotted for different values of the shape parameter α

590

591 Figure 16: Modeling of GSD: (a) model comparison with three GSDs and difference between
592 computed and measured GSDs of (b) Figure 4a (78 GSDs) and (c) Figure 4b (43 GSDs)

593

594 Figure 17: Normal distribution of $D_{50}/\langle D_{50} \rangle$ plotted for different values of the standard
595 deviation σ

596

597 Figure 18: Beta function of F_s plotted for different values of the shape parameters x_1 and x_2

598

599 Figure 19: Comparison of the results of the Monte Carlo simulation (curves) with the Figure
600 11b data (Box plots), for (a) constant α -values; (b) transport state-dependent α and several
601 values of $\langle D_{50} \rangle$; (c) several combinations of α , σ_D , and x_1 with $\langle \tau^* \rangle / \langle \tau_c^* \rangle$, $\langle D_{84} \rangle$ and $\langle S \rangle$
602 linked by relationships illustrated in Figure 3 and Figure 7.

603

604 Figure 20: Bedload computation with the *Wilcock and Crowe* [2003] equation with and without
605 taking into account the variance in bed and flow parameters ($q_s(\tau)$ and $q_s(\langle \tau \rangle)$, respectively):
606 example of the Lochsa River

607

608 Figure 21: Distribution of local transport stages τ/τ_c , for different mean transport stages
609 $\langle \tau \rangle / \langle \tau_c \rangle$

610

611

612

613

614 **NOTATIONS**

- 615 d Flow depth [m]
- 616 D_x Grain diameter (subscript denotes % finer) [m]
- 617 F_s Sand fraction at the bed surface [-]
- 618 $\langle P \rangle$ Width averaged value of parameter P : $\langle P \rangle = \frac{1}{W} \int_{y=0}^W P dy$
- 619 Q Flow discharge [m^3/s]
- 620 q Specific discharge ($q=Q/W$) [$\text{m}^3/\text{s}/\text{m}$]
- 621 Q_s Sediment discharge at equilibrium flow condition [kg/s]
- 622 q_s Bedload transport rate per unit width ($q_s=Q_s/W$) [$\text{kg}/\text{s}/\text{m}$]
- 623 R Hydraulic radius [m]
- 624 S Slope [m/m]
- 625 s Relative density ($s=\rho_s/\rho$) [-]
- 626 U Vertically averaged flow velocity [m/s]
- 627 u^* Shear velocity: $u^* = \sqrt{\tau/\rho}$ [m/s]
- 628 W Channel width [m]
- 629 x_1, x_2 Parameters of the beta distribution for F_s
- 630 α Parameter of the gamma function for τ
- 631 ξ Coefficient in $\alpha = \xi \langle \tau^* \rangle / \langle \tau^* \rangle$
- 632 σ_D Standard deviation of the normal distribution for D_{50}
- 633 σ_{DR} Standard deviation of the normal distribution for D_{84}/D_{50}
- 634 Φ Dimensionless transport rate: $\Phi = q_{sv} / [g(s-1)D^3]^{0.5}$ [-]
- 635 ρ Fluid density [kg/m^3]
- 636 ρ_s Sediment density [kg/m^3]
- 637 τ Bed shear stress [N/m^2]

638 τ^* Shields parameter calculated for diameter D_x []: $\tau^*_x = \tau/[(\rho_s - \rho)gD_x]$ [-]

639 τ^*_c Critical Shields stress corresponding to grain entrainment [-]

640

641 **APPENDIX**

Appendix A: Main characteristics of the additional data

Site	Data source	Measurement technique*	W (m)	S ($\times 10^3$)	Q (m^3/s)	U (m)	d (m)	D_{50}^{**} (mm)	D_{84}^{**} (mm)	Nb of values
Mondego River	Da Cunha [1969] in Brownlie, 1981	No information	70–189	0.54–0.97	29–660	NA	0.45–2.45	2.2–2.6	4.7–6	219
Mountain Creek	Einstein [1944] in Brownlie [1981]	Sediment discharge measured by trapping sediment in a mesh-covered hopper and pumping it into a weighing tank. Continuous water stage record. Discharge calculated from velocity (and depth) determined by means of floats.	3.3–4.3	1.36–3.15	0.1–1.5	NA	0.04–0.44	0.3–0.9	0.4–1.7	100
Saskatchewan River	Samide [1971] in Brownlie [1981]	Basket-type bed-load samplers, local velocity and depth measurements	3–6.1	1.53–7.45	4.7–39.1	NA	0.73–2.74	1.5–7.5	22.8–178	55
Hii River	Shinohara and Tsubaki [1959] in Brownlie [1981]	No information	0.8–8	0.84–1.72	0.05–4.9	NA	0.11–0.73	1.3–1.5	2.7–3.2	23
Nile River	Gaweesh and Van Rijn [1994]; Abdel-Fattah et al. [2004]	Nozzle (width = 0.096 m; height = 0.055 m; length = 0.085 m; rear width = 0.105 m; rear height = 0.06 m) connected to a nylon bag with a mesh size of 150 or 250 10^{-6} m. Velocity and depth measurements.	200–578	0.04–0.09	NA	0.4–0.9	2.76–5.72	0.3–0.6	0.3–1.7	29
Rhine River	Gaweesh and Van Rijn [1994]	Same as Nile River	300–350	0.08–0.11	NA	0.5–1.3	4.5–7.4	0.9	1.9	12
Turkey brook at Birkie Reach	Reid and Frostick [1986]	Three independent pit traps	3	2.6–16.2	0.1–13.8	NA	0.064–0.93	22	42	206
SF Cache la Poudre	Ryan et al [2005]	Helley-Smith sampler, velocity with Price AA or current meter	7.3–15.1	7	0.5–16.6	0.33–1.73	0.16–0.64	68	115	89
Cache Creek	Ryan et al [2005]	Same as SF Cache la Poudre	5.1–5.3	21	0.7–2.7	0.5–1.1	0.30–0.48	46	115	60
Coon Creek	Ryan et al [2005]	Same as SF Cache la Poudre	4.5–6.7	31	0.3–4	0.5–1.7	0.15–0.39	83	215	88
East Fork Encampt.	Ryan et al [2005]	Same as SF Cache la Poudre	3.9–6.5	38	0.1–2.2	0.3–1.14	0.10–0.34	50	133	84
Halfmoon Creek	Ryan et al [2005]	Same as SF Cache la Poudre	8.3–9.6	9.2–16	0.5–10.8	0.35–1.75	0.16–0.59	62	108	155
East Fork San Juan	Ryan et al [2005]	Wading version of an Elwha	15–17.2	8	2.8–13.8	0.71–1.59	0.27–0.52	50	112	77

Mid Fork Piedra	Ryan et al [2005]	bedload sampler, 102×203mm Same as East Fork SJ	11.4– 13.8	9–19	1–10.9	0.45–1.63	0.19–0.53	80	210	86
Silver Creek	Ryan et al [2005]	Same as East Fork SJ	3.8–4.4	45	0.1–1.4	0.08–0.39	0.11–0.32	31	73	57
Upper Florida	Ryan et al [2005]	Same as East Fork SJ	11.3–17	1.2–15.1	1.1–15.3	0.27–1.35	0.41–0.89	210	550	37
Redwood at Orick	Madej and Ozaki [1996] and unpublished USGS data	Qs (Helley-Smith sampler) and Q measured at Orick gauging station. W(Q), D ₅₀ and D ₈₄ from unpublished data	11.7–70	1.4	1.8–569	NA	NA	5	18	221
Fraser river at Agassiz	McLean et al [1999], Ferguson and Church [2009]	Basket sampler (610×255 mm) for high flows (>7000 cm) and half-size VuV sampler (225×115 mm) for lower flows. Discharge measured at gauging station.	510	0.46	1085–11445	NA	NA	42	70	76
Harris Cr.	Church and Hassan [2002]; Hassan and Church [2001]; Sterling and Church [2002]	Sediment trap	15	13	4.2–18.4	NA	NA	70	100	22
Tordera River	García and Sala [1998], Garcia et al [2000]	Pit trap	5.5	20	2–7.5	0.9–1.63	0.27–0.45	50	170	220
Bridge Cr.	Nanson [1974]	Basket sampler 38 cm long/30 cm wide, mesh size 6.4 mm, current meter and water stage recorder	2.3	67	0.3–1.1	NA	NA	30	63	18
Virginio Cr.	Tacconi and Billi [1987], Cencetti et al., [1994]	Vortex tube Bedload values deduced from graph reading	12	8	0.6–7.1	NA	NA	27	55	99
Fall River FR1	Pitlick [1993].	Helley-Smith 76 mm, water stage record and calibration with a current meter	9	3.2	0.92–10.71	0.34–1.37	0.30–0.87	11	20	175
Fall River FR2	Pitlick [1993]	Same as FR1	7	1.5	1.13–9.97	0.44–1.11	0.36–1.39	1	3	182
Torrent Saint-Pierre (braided river)	Meunier et al [2006]	U with propeller CM OTT, HS 15*15cm, Net mesh 0.25mm.	9.2–11	25	0.05–0.91*	0.48–1.98	0.08–0.98	21	80	224

642 *Discharge per unit width q [m³/s/m] ** Measured at the bed surface

643

644 **Appendix B1: 1D Equation for uniform sediments (Recking, 2010)**

$$\Phi = 0.00005 \left(\frac{\tau^*}{\tau_c^*} \right)^{12.9} \quad \text{for } \tau^*/\tau_c^* < 2.3S^{0.08} \quad (\text{B1})$$

$$\Phi = 14\tau^{*2.5} \quad \text{for } \tau^*/\tau_c^* > 2.3S^{0.08}$$

645 With $\Phi = \frac{q_s}{\rho_s \sqrt{g(s-1)D_{50}^3}}$, $\tau_c^* = 0.15S^{0.275}$

646

647 **Appendix B2: Wilcock and Crowe [2003] bedload equation**

$$W_i^* = \begin{cases} 0.002\phi^{7.5} & \text{for } \phi < 1.35 \\ 14 \left(1 - \frac{0.894}{\phi^{0.5}} \right)^{4.5} & \text{for } \phi \geq 1.35 \end{cases} \quad (\text{B2})$$

648 With

649 $W_i^* = \frac{(s-1)gq_{bi}}{f_i u_*^3}$ and $\phi = \frac{\tau}{\tau_{ri}}$

650 $\tau = 17(SD_{65})^{1/4} U^{3/2}$ (D_{65} in mm)

651 $\tau_{ri} = \tau_{r50} \left(\frac{D_i}{D_{s50}} \right)^b$

652 $b = \frac{0.67}{1 + \exp\left(1.5 - \frac{D_i}{D_{sm}}\right)}$

653 $\tau_{rm} = (s-1)\rho g D_{sm} (0.021 + 0.015 \exp[-20F_s])$

654 Where q_{vi} is the volumetric transport rate of size i per unit width ($q_v = \sum q_{vi}$), D_{sm} is the
655 geometric mean particle diameter of the bed surface and F_s is the sand fraction at the bed
656 surface.

657

658 **Appendix B3: Recking (2013)**

$$\Phi(\tau^*) = 14\tau_{D84}^{*2.5} / [1 + (\tau_m^* / \tau_{D84}^*)^4] \quad (\text{B3})$$

659 With $\Phi = \frac{q_s}{\rho_s \sqrt{g(s-1)D_{84}^3}}$, $\tau_m^* = (5S + 0.06)(D_{84} / D_{50})^{4.4\sqrt{S}-1.5}$ for gravel and 0.045 for sand.

660 $\tau_{D84}^*(R) = RS / [(s-1)D_{84}]$ or $\tau_{84}^*(q) = \frac{S}{(s-1)D_{84} [2/W + 74p^{2.6}(gS)^p q^{-2p} D_{84}^{3p-1}]}$

661 where $q = Q/W$ and where $p = 0.23$ when $q / \sqrt{gSD_{84}^3} < 100$ and $p = 0.3$ otherwise.

662
663
664
665

TABLES

Run	Fs* (x100)	D ₅₀ * (mm)	D ₈₄ * (mm)	Slope (x10 ³)	q (m ² /s)	d (m)	q _s (g/m/s)
BOMC	37.9-59.6	0.5-2.8	8-14.9	0.6-16.2	0.029-0.095	0.09-0.12	0.002-572
J27	15.5-27.7	4-5.5	16.4-20.2	2.1-17	0.05-0.13	0.09-0.11	0.003-779
J21	3.4-16.5	5.5-8	18-21.8	3.3-18.5	0.065-0.126	0.1-0.12	0.017-152
J14	0.6-1.8	9-12	21.4-23.2	5.2-18.6	0.079-0.133	0.102-0.12	0.019-115
J06	0-0.3	10.5-12.9	20.4-24.8	4.5-22.5	0.078-0.133	0.1-0.11	0.000-204

666
667
668
669
670

* measured at the bed surface
Table 1: Experimental runs from Wilcock et al 2001

Parameter	Range
Slope (m/m)	0.00004–0.085
Diameter D ₅₀ (mm)	0.25–220
Diameter D ₈₄ (mm)	0.3–558
Bankfull depth (m)	0.04–7.5
Bankfull width (m)	0.3–578

671
672
673
674
675
676
677

Table 2: Main characteristics of field data

Class	i (%)	D _i (mm)	C _n	Remark
0	100F _s	D _m	-	D _m = 2mm but if F _s = 0 D _m = the minimum diameter of the GSD
1			16	
2	$\frac{50-100F_s}{C_n} + 100F_s$	$\frac{D_{50} - D_m}{C_n} + D_m$	3.3	3.3 replaced by 8 if D _m > 2 mm
3			1.9	
4			1.3	
5	50	D ₅₀	-	
6	60	$\frac{D_{84} - D_{50}}{C_n} + D_{50}$	5.9	
7	70		2.3	
8	84	D ₈₄	-	
9	90		1.3	
10	98	C _n D ₈₄	2.5	2.5 replaced by 1.5 if D _m > 2 mm
11	100		5.1	

678
679
680
681
682
683
684

Table 3: Grain Size distribution Model. Input data are D₅₀, D₈₄, F_s (the sand fraction), and D_m if F_s=0 (minimum grain size). C_n is a coefficient and D_i is the upper limit of the size class. For constructing a GSD, F_s and C_n are used for computing the limits of each size class (column 3) and the % in each class (column 2).

685 **REFERENCES**

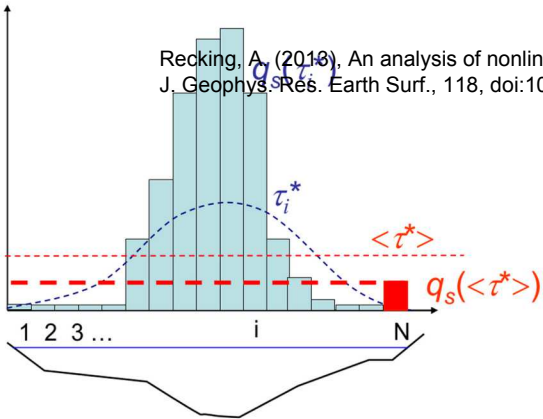
- 686 Abdel-Fattah, S., A. Amin, and L. C. Van Rijn (2004), Sand transport in Nile river, Egypt,
687 *Journal of Hydraulic Engineering*, 130, 488-500.
- 688 Andrews, E. D. (1983), Entrainment of gravel from naturally sorted riverbed material,
689 *Geological Society of America Bulletin*, 94, 1225-1231.
- 690 Barkett, B. L. (1998), The relationship between grain size and shear stress in two gravel bed
691 streams, Univ. of Colo., Boulder, CO.
- 692 Barry, J. J., J. M. Buffington, P. Goodwin, J. G. King, and W. W. Emmett (2008),
693 Performance of bedload transport equations relative to geomorphic significance: predicting
694 discharge and its transport rate, *Journal of Hydraulic Engineering (ASCE)*, 134, 601-615.
- 695 Barry, J. J., J. M. Buffington, and J. G. King (2004), A general power equation for predicting
696 bed load transport rates in gravel bed rivers, *Water Resources Research*, 40, 1-22.
- 697 Barry, J. J., J. M. Buffington, and J. G. King (2007), Correction to "A general power equation
698 for predicting bed load transport rates in gravel bed rivers", *Water Resources Research*, 43.
- 699 Bathurst, J. C. (2007), Effect of coarse surface layer on bed-load transport, *Journal of*
700 *Hydraulic Engineering (ASCE)*, 133, 1192-1205.
- 701 Bertoldi, W., P. Ashmore, and M. Tubino (2009), A method for estimating the mean bed load
702 flux in braided rivers, *Geomorphology*, 103, 330-340.
- 703 Brownlie, W. R. (1981), Computation of alluvial channel data: Laboratory and Field, 213 pp,
704 California Institute of Technology, Pasadena, California.
- 705 Buffington, J. M. (2000), The legend of A. F. Shields (Closure), *Journal of Hydraulic*
706 *Engineering*, 126, 721-723.
- 707 Buffington, J. M. (2012), Changes in channel morphology over human time scales, in *Gravel-*
708 *bed Rivers: Processes, Tools, Environments*, edited by M. Church, Biron, P.M., Roy, A.G.
709 (Eds.), pp. 435–463., Wiley, Chichester, UK.
- 710 Buffington, J. M., and D. R. Montgomery (1997), A systematic analysis of eight decades of
711 incipient motion studies, with special reference to gravel-bedded rivers, *Water Resources*
712 *Research*, 33, 1993-2027.
- 713 Buffington, J. M., and D. R. Montgomery (1999a), Effects of hydraulic roughness on surface
714 textures of gravel-bed rivers, *Water Resources Research*, 35, 3507.
- 715 Buffington, J. M., and D. R. Montgomery (1999b), A procedure for classifying textural facies
716 in gravel-bed rivers, *Water Resources Research*, 35, 1903.
- 717 Bunte, K., and S. R. Abt (2001), Sampling surface and subsurface particle-size distributions
718 in Wadable and cobble bed streams for analyses in sediment transport, hydraulics and
719 streambed monitoring, 450 pp, USDA Report RMRS-GTR-74.
- 720 Cencetti, C., P. Tacconi, M. Del Prete, and M. Rinaldi (1994), Variability of gravel movement
721 on the Virginio gravel-bed stream (central Italy) during some floods, paper presented at
722 Variability in Stream Erosion and Sediment Transport (Proceedings of the Canberra
723 Symposium December 1994). IAHS Publ. no. 224.3-11
- 724 Chiari, M., and D. Rickenmann (2010), Back-calculation of bedload transport in steep
725 channels with a numerical model, *Earth Surface Processes and Landforms*, 36, 805-815.
- 726 Church, M., and M. A. Hassan (2002), Mobility of bed material in Harris Creek, *Water*
727 *Resources Research*, 38, 19-31.
- 728 Church, M., and R. Kellerhalls (1978), On the statistics of grain size variation along a gravel
729 bed river, *Can. J. Earth Sci.*, 15, 1151-1160.
- 730 Church, M., and A. Zimmerman (2007), Form and stability of step-pool channels: Research
731 progress, *Water Resources Research*, 43, 1-21.
- 732 Crowder, D. W., and P. Diplas (1997), Sampling heterogeneous deposits in gravel-bed
733 streams, *Journal of Hydraulic Engineering*, 123, 1106-1117.

- 734 Da Cunha, L. V. (1969), River Mondego, Portugal," Personal Communication, Laboratorio
735 Nacional De Engenharia Civil, Lisboa (Published in Peterson, A. W. , and Howells , R. F. ,
736 "A Compendium of Solids Transport Data for Mobile Boundary Channels," Report No. HY-
737 1973-ST3, Department of Civil Engineering, University of Alberta, Canada, January 1973).
738 edited.
- 739 Dietrich, W. E., J. W. Kirchner, H. Ikeda, and F. Iseya (1989), Sediment supply and the
740 development of the coarse surface layer in gravel-bedded rivers, *Nature*, 340, 215-217.
- 741 Dietrich, W. E., P. A. Nelson, E. Yager, J. G. Venditti, M. P. Lamb, and L. Collins (2006),
742 Sediment patches, sediment supply and channel morphology, in *In: River, Coastal and*
743 *Estuarine: Morphodynamics*, Parker, G., and Garcia, M. H. (Eds.), Taylor and
744 Francis/Balkema, Lisse, The Netherlands, edited, pp. 79-90.
- 745 Einstein, H. A. (1944), Bed Load Transportation in Mountain Creek," U.S. Soil Conservation
746 Service, SCS-TP-55, 50pp.
- 747 Einstein, H. A. (1950), The bed-load function for sediment transportation in open channel
748 flows, 71 pp, United States Department of Agriculture - Soil Conservation Service,
749 Washington.
- 750 Ferguson, R. (2007), Flow resistance equations for gravel and boulder bed streams, *Water*
751 *Resources Research*, 43, 1-12.
- 752 Ferguson, R. (2012), River channel slope, flow resistance, and gravel entrainment thresholds,
753 *Water Resour. Res.*, 48, 1-13.
- 754 Ferguson, R., and M. Church (2009), A critical perspective on 1-D modeling of river
755 processes: Gravel load and aggradation in lower Fraser River, *Water Resour. Res.*, 45.
- 756 Ferguson, R. I. (2003), The missing dimension: effects of lateral variation on 1-D calculations
757 of fluvial bedload transport, *Geomorphology*, 56, 1-14.
- 758 Francalanci, S., L. Solari, M. Toffolon, and G. Parker (2012), Do alternate bars affect
759 sediment transport and flow resistance in gravel bed rivers?, *Earth Surface Processes and*
760 *Landforms*, 37, 866-875.
- 761 Gaeuman, D., E. D. Andrews, A. Krause, and W. Smith (2009), Predicted fractional bed load
762 transport rates: Application of the Wilcock-Crowe equations to a regulated gravel bed river,
763 *Water Resour. Res.*, 45, 1-15.
- 764 Garcia, C., J. B. Laronne, and M. Sala (2000), Continuous monitoring of bedload flux in a
765 mountain gravel-bed river, *Geomorphology*, 34, 23-31.
- 766 García, C., and M. Sala (1998), Application de formulas de transporte de fondo a un rio de
767 gravas: comparacion con las tasas reales de transporte en el rio tordera, *Ingeniería del Agua*,
768 5, 59-72.
- 769 Gaweesh, M. T. K., and L. C. Van Rijn (1994), Bed-load sampling in sand-bed rivers, *Journal*
770 *of Hydraulics Engineering*, 120, 1364-1384.
- 771 Gomez, B., and M. Church (1989), An assessment of bedload sediment transport formulae for
772 gravel bed rivers, *Water Resources Research*, 25, 1161-1186.
- 773 Habersack, H. M., and J. B. Laronne (2002), Evaluation and improvement of bed load
774 discharge formulas based on Helley-Smith sampling in an Alpine gravel bed river, *Journal of*
775 *Hydraulic Engineering*, 128, 484-499.
- 776 Hassan, M. A., and M. Church (2001), Sensitivity of bed load transport in Harris Creek:
777 Seasonal and spatial variation over a cobble-gravel bar, *Water Resources Research*, 37, 813.
- 778 King, J. G., W. W. Emmett, P. Whiting, S. T. Kenworthy, and J. J. Barry (2004), Sediment
779 transport data and related information for selected coarse-bed streams and rivers in Idaho,
780 (<http://www.fs.fed.us/rm/boise/research/watershed/BAT/>).
- 781 Lamb, M. P., W. E. Dietrich, and J.-G. Venditti (2008), Is the critical Shields stress for
782 incipient sediment motion dependent on channel-bed slope?, *J. Geophys. Res.*, 113.

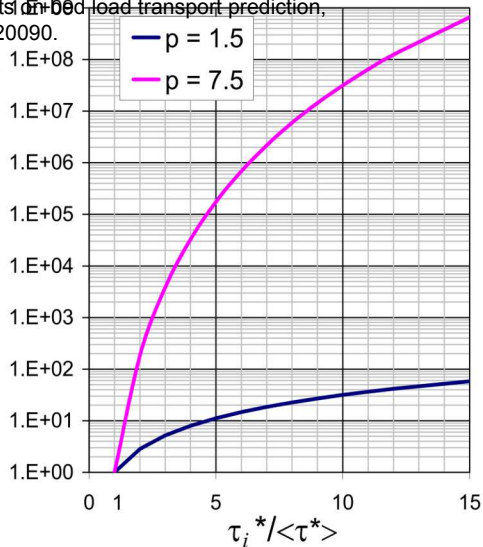
- 783 Madej, M. A., and V. Ozaki (1996), Channel response to sediment wave propagation and
784 movement, Redwood Creek, California, USA, *Earth Surface Processes and Landforms*, 21,
785 911-927.
- 786 McLean, D. G., M. Church, and B. Tassone (1999), Sediment transport along lower Fraser
787 River, 1, Measurements and hydraulic computations, *Water Resources Research*, 35, 2533-
788 2548.
- 789 Meunier, P., F. Metivier, E. Lajeunesse, A. S. Meriaux, and J. Faure (2006), Flow pattern and
790 sediment transport in a braided river: The "torrent de St Pierre" (French Alps), *Journal of*
791 *Hydrology*, 330, 496-505.
- 792 Meyer-Peter, E., and R. Mueller (1948), Formulas for bed-load transport, paper presented at
793 Proceedings 2d Meeting IAHR, Stockholm.39-64
- 794 Montgomery, D. R., and J. M. Buffington (1997), Channel-reach morphology in mountain
795 drainage basins, *Geological Society of America Bulletin*, 109, 596-611.
- 796 Mueller, E. R., J. Pitlick, and J. M. Nelson (2005), Variation in the reference Shields stress for
797 bed load transport in gravel-bed streams and rivers, *Water Resources Research*, 41, W04006
798 (04001-04010).
- 799 Nanson, G. C. (1974), Bedload and suspended-load transport in a small, steep, mountain
800 stream, *Am. J. Sci*, 274, 471-486.
- 801 Nicholas, A. P. (2000), Modelling bedload yield in braided gravel bed rivers,
802 *Geomorphology*, 36, 89-106.
- 803 Paola, C. (1996), *Incoherent structures: turbulence as a metaphor for stream braiding*, 706-
804 723 pp., In Ashworth, P.J., Bennet, S.J., Best, J.L., McLelland, S.J. (Eds), John Wiley and
805 sons.
- 806 Paola, C., and R. Seal (1995), Grain size patchiness as a cause of selective deposition and
807 downstream fining, *Water Resources Research*, 31, 1395-1408.
- 808 Parker, G. (1978), Self-formed straight rivers with equilibrium bank and mobile bed. Part 2 :
809 the gravel river, *Journal of Fluid mechanics*, 89, 127-146.
- 810 Parker, G. (1990), Surface-based bedload transport relation for gravel rivers, *Journal of*
811 *Hydraulic Research*, 28, 417-428.
- 812 Parker, G. (2009), Transport of gravel and sediment mixtures, in *ASCE Manual 54*
813 *"Sedimentation Engineering"*, edited by ASCE.
- 814 Parker, G., and P. C. Klingeman (1982), On why gravel bed streams are paved, *Water*
815 *Resources Research*, 18, 1409-1423.
- 816 Parker, G., P. C. Klingeman, and D. G. McLean (1982), Bedload and size distribution in
817 paved gravel-bed streams, *Journal of the Hydraulics Division (ASCE)*, 108, 544-571.
- 818 Parker, G., G. Seminara, and L. Solari (2003), Bed load at low Shields stress on arbitrarily
819 sloping beds: Alternative entrainment formulation, *Water Resources Research*, 39, 1183.
- 820 Parker, G., P. R. Wilcock, C. Paola, W. E. Dietrich, and J. Pitlick (2007), Physical basis for
821 quasi-universal relations describing bankfull hydraulic geometry of single-thread gravel bed
822 rivers, *J. Geophys. Res.*, 112, F04005.
- 823 Pitlick, J. (1993), Response and recovery of a subalpine stream following a catastrophic flood,
824 *Geological Society of America Bulletin*, 105, 657-670.
- 825 Pitlick, J., E. R. Mueller, C. Segura, R. Cress, and M. Torizzo (2008), Relation between flow,
826 surface layer armoring and sediment transport in gravel bed rivers, *Earth Surface Processes*
827 *and Landforms*, 33, DOI:10.1002/esp.1607, 1192-1209.
- 828 Recking, A. (2009), Theoretical development on the effects of changing flow hydraulics on
829 incipient bedload motion, *Water Resources Research*, 45, W04401, 16.
- 830 Recking, A. (2010), A comparison between flume and field bedload transport data and
831 consequences for surface based bedload transport prediction, *Water Resources Research*, 46,
832 1-16.

- 833 Recking, A. (2012), Influence of sediment supply on mountain streams bedload transport
834 rates, *Geomorphology*, 12 p.
- 835 Recking, A. (2013), A simple method for calculating reach-averaged bedload transport,
836 *Journal of Hydraulic Engineering*, 139.
- 837 Recking, A., P. Frey, A. Paquier, P. Belleudy, and J. Y. Champagne (2008), Feedback
838 between bed load and flow resistance in gravel and cobble bed rivers, *Water Resources*
839 *Research*, 44, 21.
- 840 Recking, A., F. Liébault, C. Peteuil, and T. Jolimet (2012), Testing several bed load transport
841 equations with consideration of time scales, *Earth Surface Processes and Landforms*.
- 842 Reid, I., and L. E. Frostick (1986), Dynamics of bedload transport in Turkey Brook, a coarse-
843 grained alluvial channel, *Earth Surface Processes and Landforms*, 11, 143-155.
- 844 Rickenmann, D. (2001), Comparison of bed load transport in torrents and gravel bed streams,
845 *Water Resources Research*, 37, 3295.
- 846 Rickenmann, D., and A. Recking (2011), Evaluation of flow resistance in gravel-bed rivers
847 through a large field dataset, *Water Resources Research*, 47, 1-22.
- 848 Ryan, S. E., L. Porth, and C. Troendle (2005), Coarse sediment transport in mountain streams
849 in Colorado and Wyoming, USA., *Earth Surface Processes and Landforms*, 30, 269-288.
- 850 Ryan, S. E., L. S. Porth, and C. A. Troendle (2002), Defining phases of bedload transport
851 using piecewise regression, *Earth Surface Processes and Landforms*, 27, 971-990.
- 852 Samide, G. W. (1971), Sediment transport measurements, PhD thesis dissertation, University
853 of Alberta.
- 854 Segura, C., J. H. McCutchan, W. M. Lewis, and J. Pitlick (2010), The influence of channel
855 bed disturbance on algal biomass in a Colorado mountain stream, *Ecohydrology*, 11.
- 856 Shinohara, K., and T. Tsubaki (1959), On the characteristics of sand waves formed upon beds
857 of the open channels and rivers, reports of Research Institute of Applied Mechanics,
858 Vol. VII, No. 25, Kyushu University.
- 859 Sterling, M. S., and M. Church (2002), Sediment trapping characteristics of a pit trap and the
860 Helley-Smith sampler in a cobble gravel bed river, *Water Resour. Res.*, 38, 1-19.
- 861 Tacconi, P., and P. Billi (1987), Bedload transport measurements by the vortex-tube trap on
862 Virginio Creek, Italy, in *Sediment transport in gravel bed rivers*, edited by C. R. Thorne,
863 Bathurst, J.C., Hey, R.D., pp. 583-606, John Wiley & Sons Ltd, Chichester.
- 864 Tunncliffe, J., M. Hicks, P. Ashmore, J. Walsh, J. T. Gardner, and M. Duncan (2012), Use of
865 2D hydraulic models to develop and improve parameterized 1D models of sediment transport
866 paper presented at EGU 2012 (Poster Session), Vienna, Austria
- 867 Wilcock, P., J. Pitlick, and Y. Cui (2009), Sediment transport primer, Estimating bed-material
868 transport in gravel-bed rivers, 78 pp, Gen Tech Rep RMRS-GTR-226. Fort Collins, CO: U.S.
869 Department of Agriculture, Forest service, Rocky Mountain Research Station.
- 870 Wilcock, P. R., and J. C. Crowe (2003), Surface-based transport model for mixed-size
871 sediment, *Journal of Hydraulic Engineering (ASCE)*, 129, 120-128.
- 872 Wilcock, P. R., S. T. Kenworthy, and J. C. Crowe (2001), Experimental study of the transport
873 of mixed sand and gravel, *Water Resources Research*, 37, 3349.
- 874 Wilcock, P. R., and B. W. McArdeell (1993), Surface-based fractional transport rates:
875 Mobilization thresholds and partial transport of a sand-gravel sediment, *Water Resources*
876 *Research*, 29, 1297-1312.
- 877 Wolman, M. G. (1954), Method of sampling coarse river bed material, *Transactions of the*
878 *American Geophysical Union*, 35, 951-956.
- 879
880

Recking, A. (2018), An analysis of nonlinearity effects on bed load transport prediction, J. Geophys. Res. Earth Surf., 118, doi:10.1002/jgrf.20090.

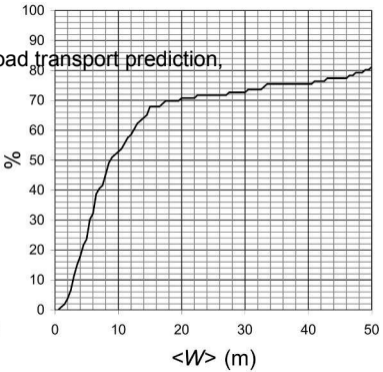
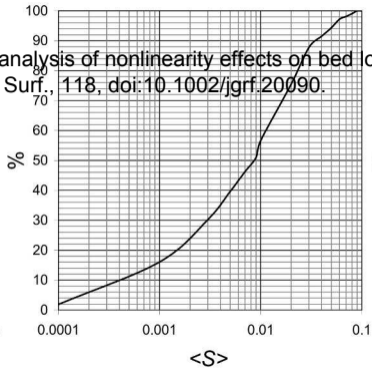
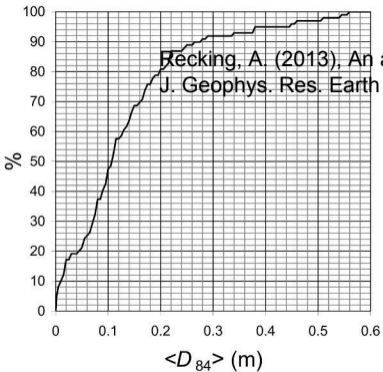


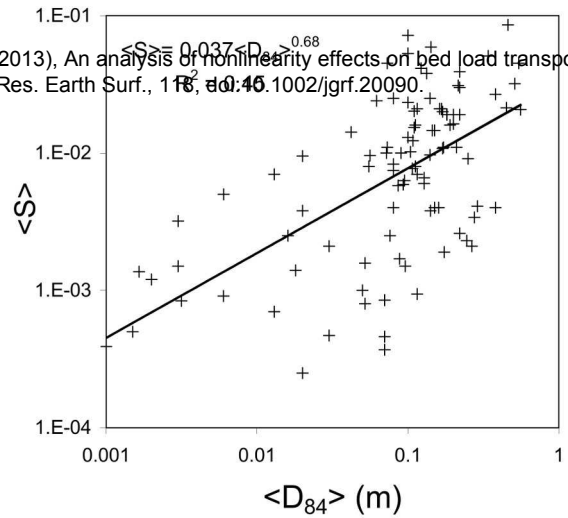
$$\overline{(\tau^*)^p}$$

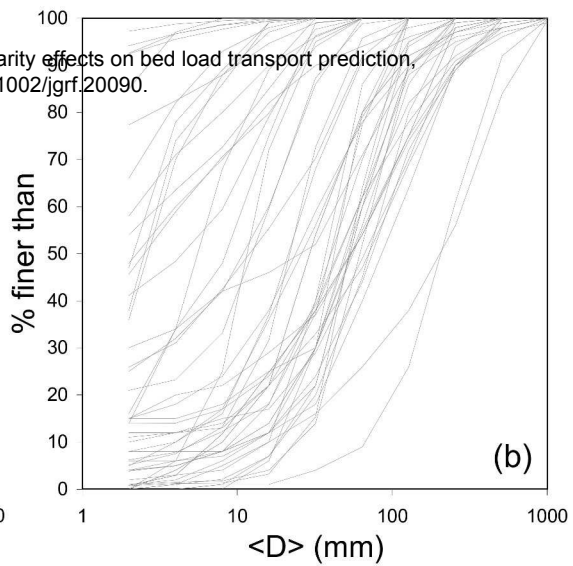
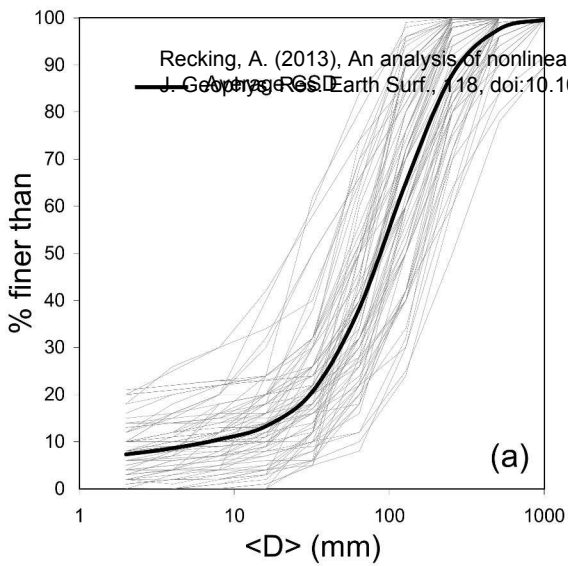


$$\langle \tau^* \rangle = \frac{1}{N} \sum_N \tau_i^*$$

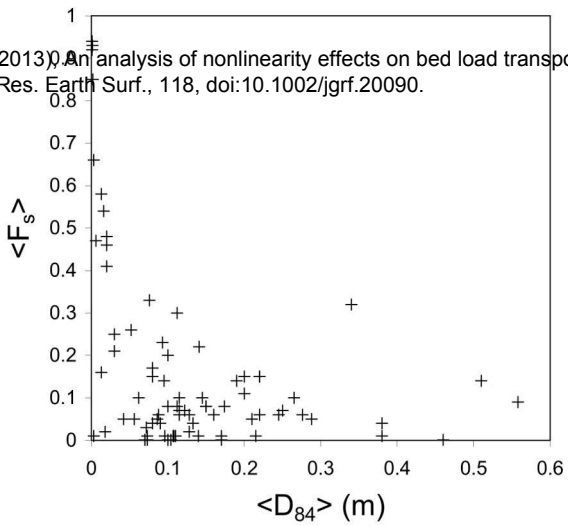
$$q_s(\langle \tau^* \rangle) < \frac{1}{N} \sum_N q_s(\tau_i^*)$$

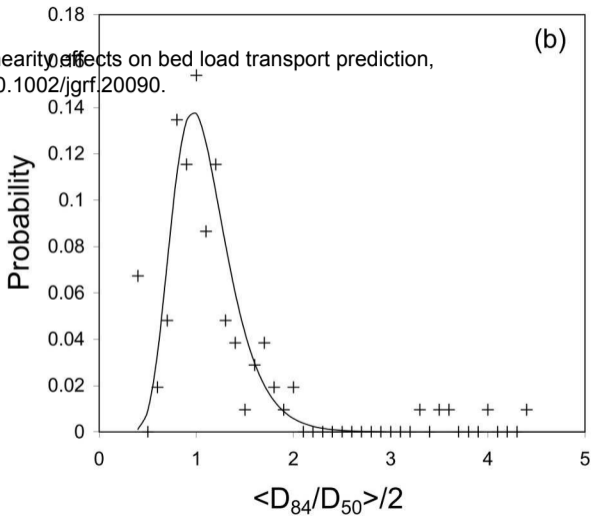
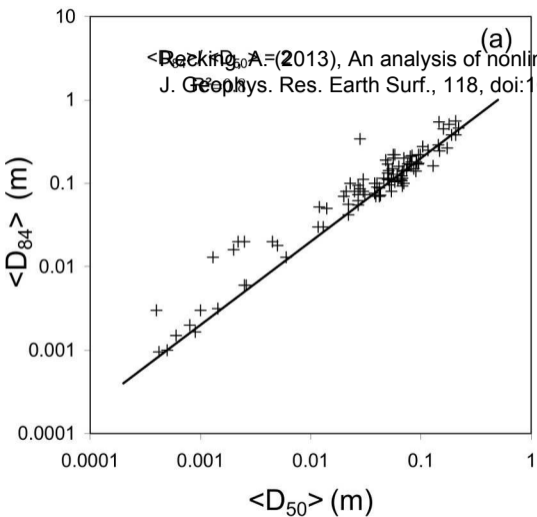




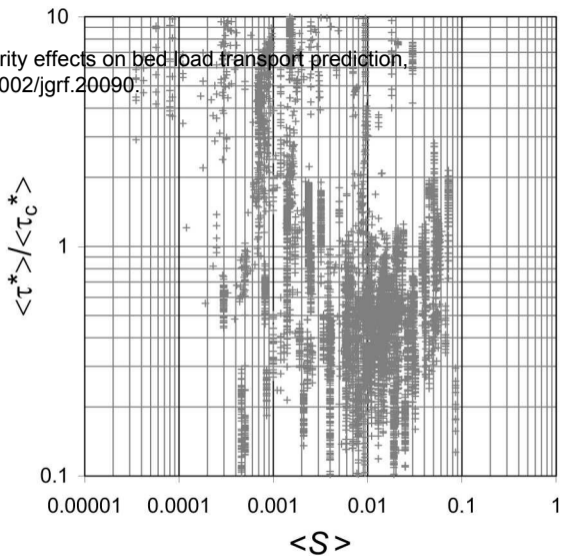
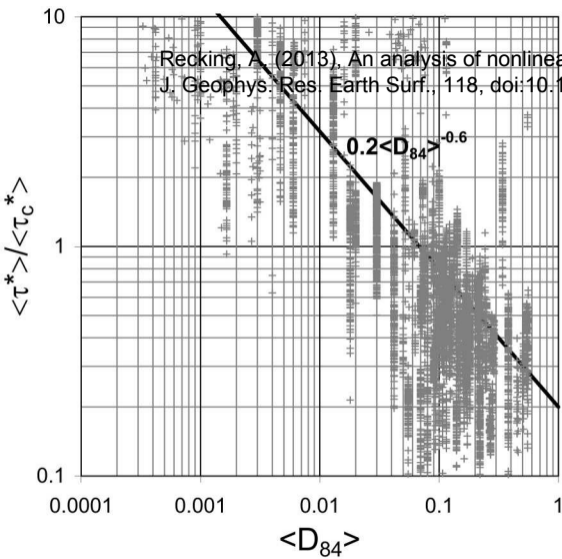


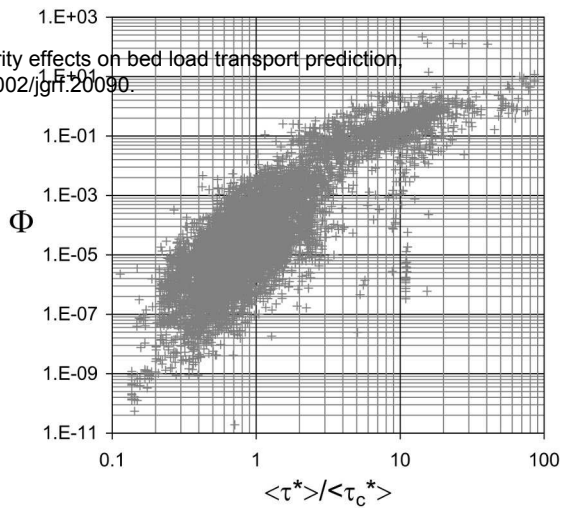
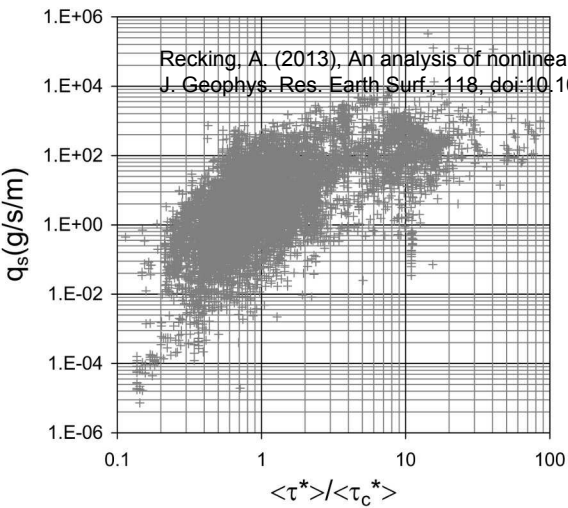
2013). An analysis of nonlinearity effects on bed load transport
Res. Earth Surf., 118, doi:10.1002/jgrf.20090.

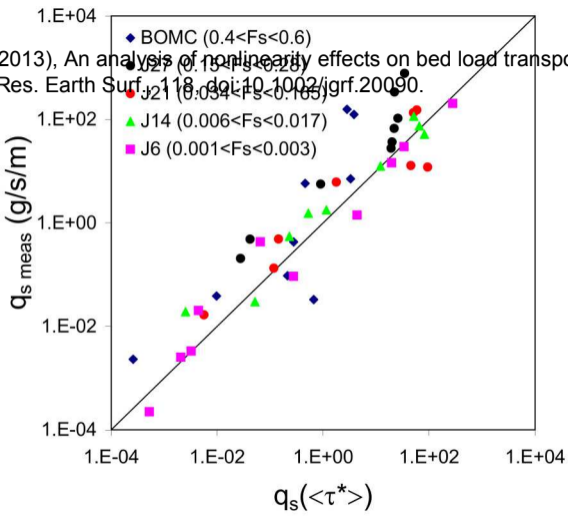


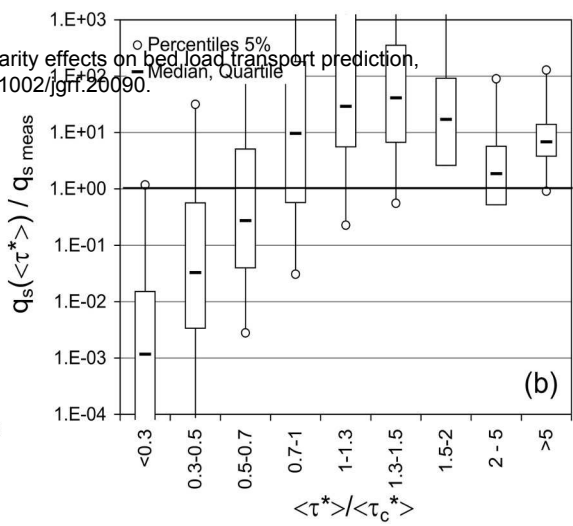
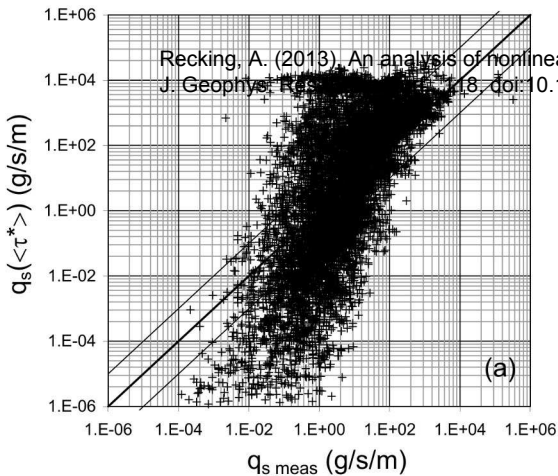


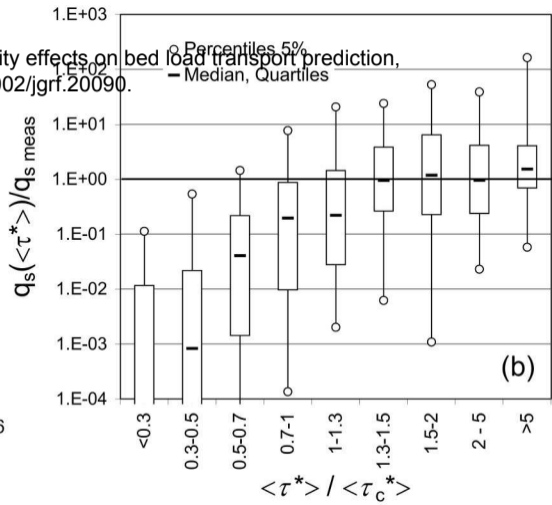
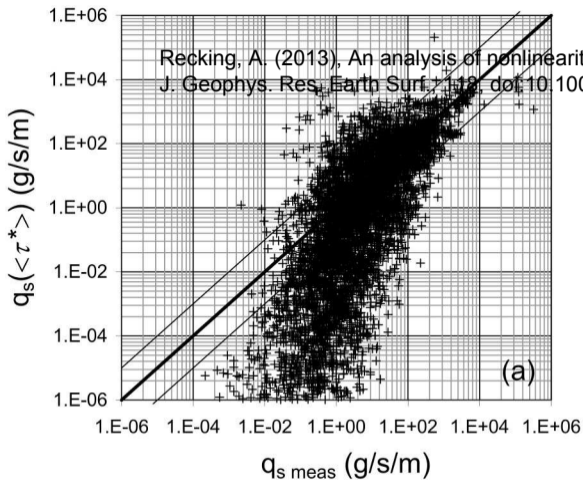
Becking, A. (2013), An analysis of nonlinearity effects on bed load transport prediction, J. Geophys. Res. Earth Surf., 118, doi:10.1002/jgrf.20090.

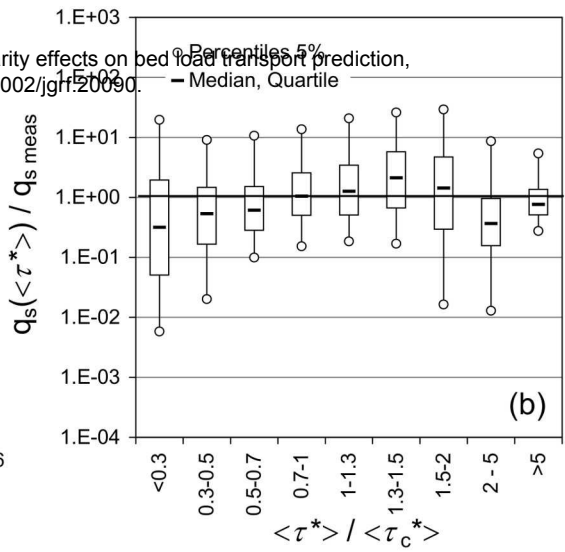
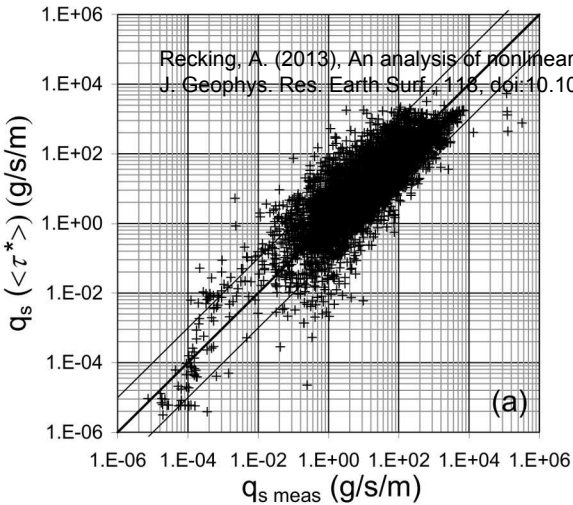


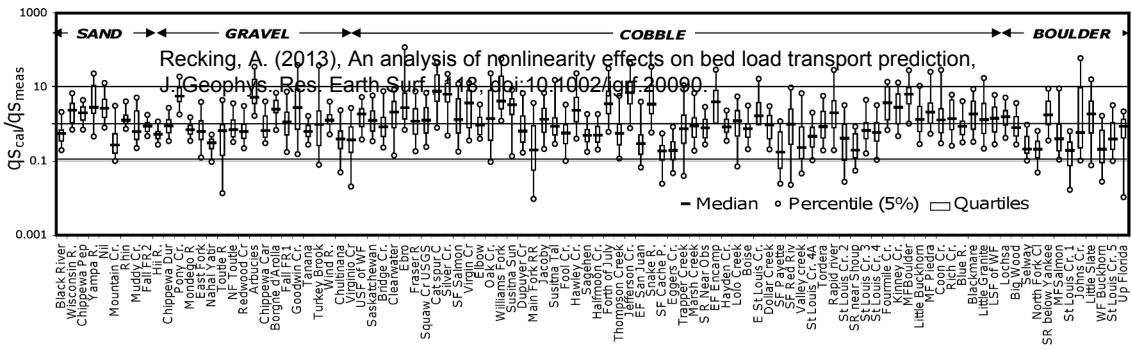


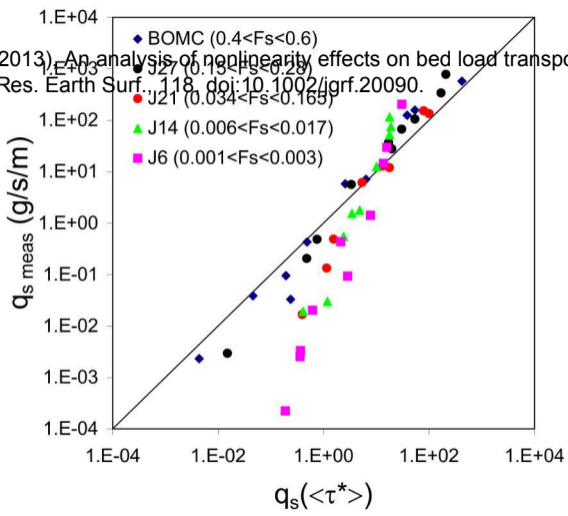


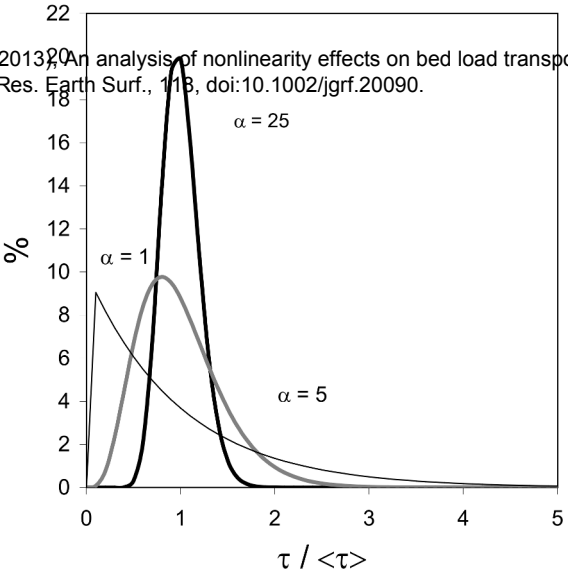


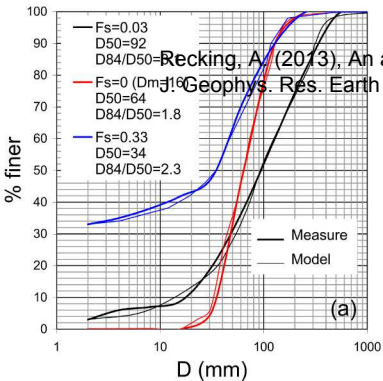




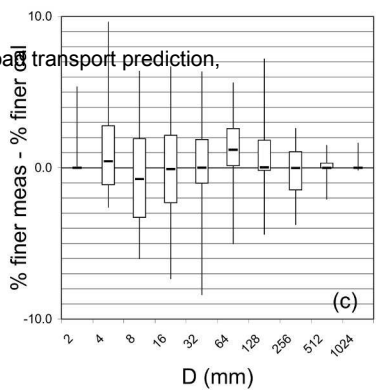
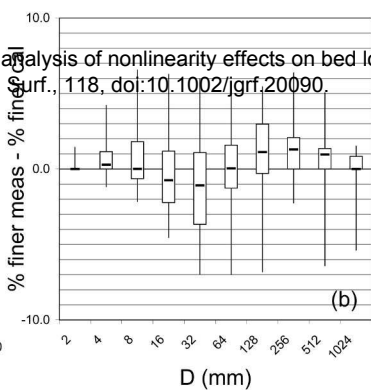




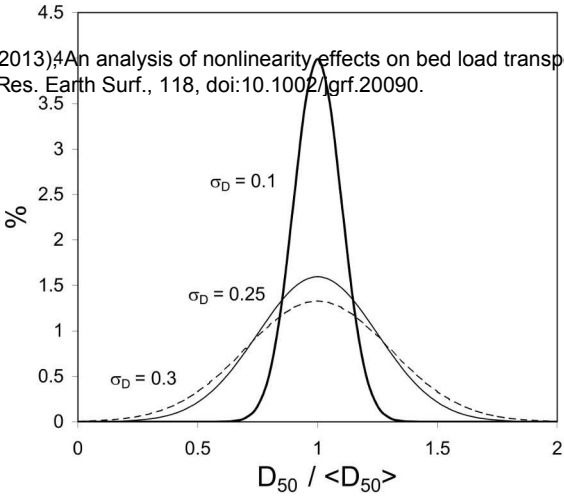




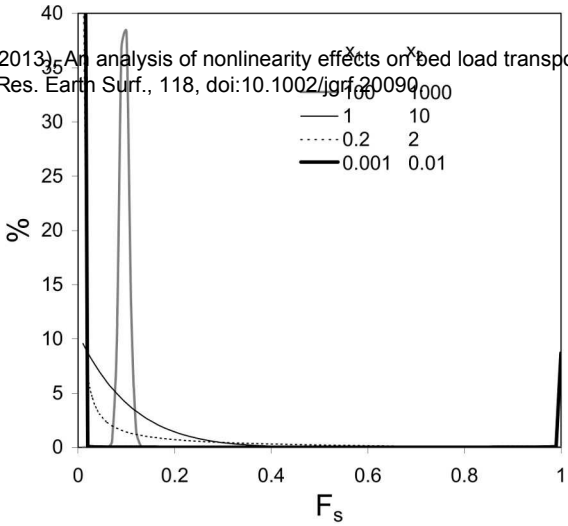
Recking, A. (2013), An analysis of nonlinearity effects on bed load transport prediction, *J. Geophys. Res. Earth Surf.*, 118, doi:10.1002/jgrf.20090.

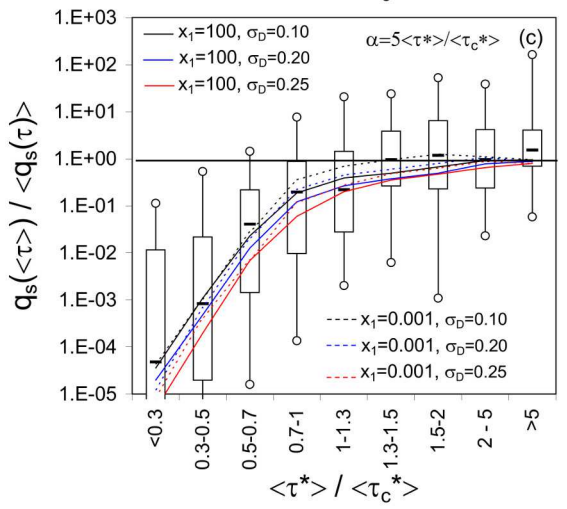
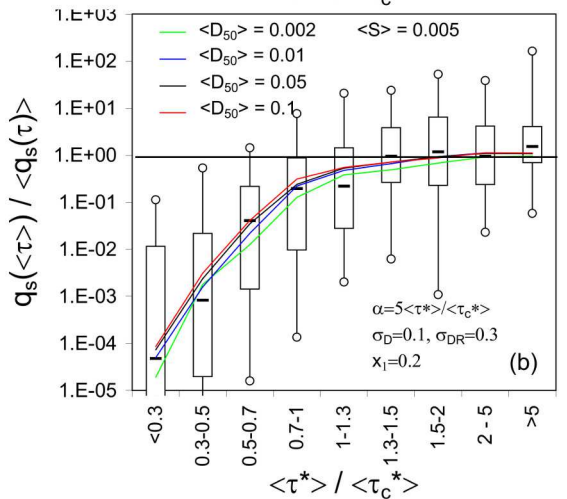
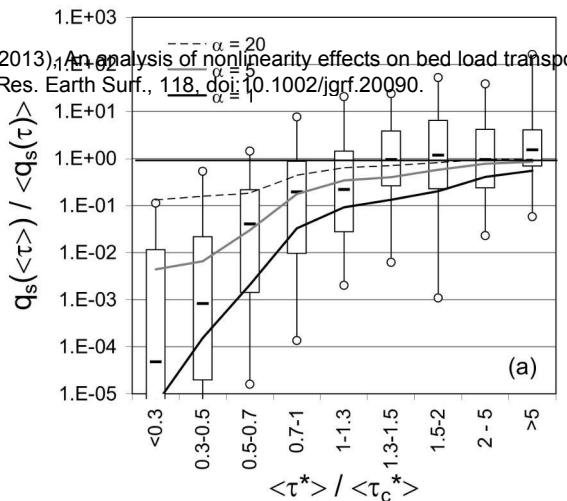


2013) An analysis of nonlinearity effects on bed load transport
Res. Earth Surf., 118, doi:10.1002/grf.20090.



2013). An analysis of nonlinearity effects on bed load transport
Res. Earth Surf., 118, doi:10.1002/jgrf.20090





2013), An analysis of nonlinearity effects on bed load transport
Res. Earth Surf., 118, doi:10.1002/jgrf.20090.

